Spatial and temporal organization of RecA in the *Escherichia coli* DNA-damage response

Harshad Ghodke[1,2], Bishnu P Paudel[1,2], Jacob S Lewis[1,2], Slobodan Jergic[1,2], Kamya Gopal[3], Zachary J Romero[3], Elizabeth A Wood[3], Roger Woodgate[4], Michael M Cox[3], Antoine M van Oijen[1,2*]

[1]School of Chemistry, University of Wollongong, Wollongong, Australia

[2] Illawarra Health and Medical Research Institute, Wollongong, Australia

[3] Biochemistry Department, University of Wisconsin-Madison, Madison, Wisconsin, United States of America

[4] Laboratory of Genomic Integrity, National Institute of Child Health and Human Development, National Institutes of Health, Bethesda, MD, USA

Correspondence:

Antoine M van Oijen, School of Chemistry, University of Wollongong, Wollongong, New South Wales, 2522, Australia

Lead contact:

Antoine M van Oijen, School of Chemistry, University of Wollongong, Wollongong, New South Wales, 2522, Australia

Summary:

The RecA protein orchestrates the cellular response to DNA damage via its multiple roles in the bacterial SOS response. Lack of tools that provide unambiguous access to the various RecA states within the cell have prevented understanding of the spatial and temporal changes in RecA structure/function that underlie control of the damage response. Here, we develop a monomeric C-terminal fragment of the λ repressor as a novel fluorescent probe that specifically interacts with RecA filaments on single-stranded DNA (RecA*). Single-molecule imaging techniques in live cells demonstrate that RecA is largely sequestered in storage structures during normal metabolism. Upon DNA damage, the storage structures dissolve and the cytosolic pool of RecA rapidly nucleates to form early SOS-signaling complexes, maturing into DNA-bound RecA bundles at later time points. Both before and after SOS induction, RecA* largely appears at locations distal from replisomes. Upon completion of repair, RecA storage structures reform.

Introduction

All cells possess an intricately regulated response to DNA damage. Bacteria have evolved an extensive regulatory network called the SOS response to control the synthesis of factors

that protect and repair the genome. Processes coordinately regulated within the SOS response include error-free DNA repair, error-prone lesion bypass, cell division, and recombination.

The RecA protein is the master regulator of SOS, with at least three distinct roles. First, RecA forms a ternary complex with single-stranded DNA (ssDNA) and ATP to form the activated RecA*. RecA* catalyzes auto-proteolysis of the transcriptional repressor LexA to induce expression of more than 40 SOS genes (Courcelle et al., 2001; Fernandez De Henestrosa et al., 2000; Kenyon and Walker, 1980; Little and Mount, 1982; Little et al., 1981). RecA* thus uses the ssDNA generated when replication forks encounter DNA lesions as an induction signal (Sassanfar and Roberts, 1990). Second, along with several other accessory proteins, RecA mediates error-free recombinational DNA repair at sites of single-strand gaps, double-strand breaks (DSBs) and failed replisomes (Cox et al., 2000; Kowalczykowski, 2000; Kuzminov, 1995; Lusetti and Cox, 2002). Third, the formation and activity of active DNA Polymerase V complex capable of lesion bypass requires RecA* (Jaszczur et al., 2016; Jiang et al., 2009; Robinson et al., 2015).

RecA is a prototypical member of a class of proteins that are critical for genomic stability across all domains of life (Baumann et al., 1996; Bianco et al., 1998; Lusetti et al., 2003a; San Filippo et al., 2008; Sung, 1994). In higher organisms, including humans, the homologous protein Rad51 supports error-free double-strand break repair by catalyzing strand exchange much like the RecA protein does in eubacteria (Baumann et al., 1996; Sung, 1994). Mutations in human Rad51 and accessory proteins have been implicated in carcinomas and Fanconi anemia (Chen et al., 2015; Kato et al., 2000; Prakash et al., 2015). Unsurprisingly, RecA and related recombinases are highly regulated, with a variety of accessory proteins governing every facet of their multiple functions (Cox, 2007). Directed-evolution approaches can be used to enhance the catalytic activities of recombinases in cells (Kim et al., 2015). However, RecA functional enhancement has a cost, disrupting an evolved balance between the various processes of DNA metabolism that share a common genomic DNA substrate (Kim et al., 2015). Many deleterious genomic events occur at the interfaces between replication, repair, recombination, and transcription.

An understanding of how organisms maintain genetic integrity requires an examination of the protein actors in their native cellular environments. In response to DNA damage, transcription of the *recA* gene is upregulated ten-fold within minutes (Courcelle et al., 2001; Renzette et al., 2005). Using immunostaining, the copy number of RecA in undamaged cells has been estimated to be about 7,000-15,000 per cell, increasing to 100,000 per cell upon triggering the DNA-damage response (Boudsocq et al., 1997; Stohl et al., 2003). Visualization of C-terminal GFP fusions of wild-type and mutant *recA* alleles placed under the native *recA* promoter in *E. coli* have revealed that RecA forms foci in cells (Lesterlin et al., 2014; Renzette et al., 2005; Renzette et al., 2007). Interpretation of the localizations observed in these experiments has been clouded by three issues: 1. fluorescent fusions of RecA have

consistently yielded loss-of-function phenotypes to RecA (Handa et al., 2009; Renzette et al., 2005), making interpretation of the localizations revealed by these tagged proteins highly challenging. 2. this issue is further complicated by the fact that fluorescent proteins do not behave as inert tags and can influence intracellular localization in bacterial cells (Ghodke et al., 2016; Ouzounov et al., 2016). Indeed, *Bacillus subtilis* RecA tagged with GFP, YFP and mRFP yielded different localizations in response to DNA damage (Kidane and Graumann, 2005). These challenges do not come as a surprise since both N- and C-terminal ends are important for RecA function and localization (Eggler et al., 2003; Lusetti et al., 2003a; Lusetti et al., 2003b; Rajendram et al., 2015). 3. at least *in vitro*, untagged RecA has a remarkable ability to self-assemble, into different complexes that form on single-stranded DNA (RecA*), on double-stranded DNA, or are free of DNA (Brenner et al., 1988; Egelman and Stasiak, 1986, 1988; Stasiak and Egelman, 1986). The properties of these assemblies are often determined by the state of hydrolysis of associated ATP. Thus, unambiguous assignment of the molecular composition of RecA features in live cells has been difficult.

In the absence of DNA, RecA can polymerize to form aggregates of various stoichiometry to yield dimers, tetramers, 'rods' and 'bundles' (Brenner et al., 1988). Some of these states may have a physiological relevance: RecA fusions with the best functionality have revealed DNA-free aggregates that are confined to the cellular poles, outside of the nucleoid and associated with anionic phospholipids in the inner membrane (Rajendram et al., 2015; Renzette et al., 2005). These DNA-free aggregates were hypothesized to be 'storage structures' of RecA, although their functionality in and relevance to the DNA damage response remain unclear.

Early electron-microscopy studies revealed that multiple dsDNA-RecA-ATPγS filaments could also associate to form structures confusingly termed as 'bundles' (Egelman and Stasiak, 1988). This study also identified that ssDNA-RecA-ATPγS filaments could aggregate together. Electron microscopy of cells revealed that RecA appeared to form 'bundles' that were aligned next to the inner membrane in cells after DNA damage (Levin-Zaidman et al., 2000). In cells carrying an additional allele of wild-type RecA at a secondary chromosomal locus to increase overall RecA function, long RecA structures called 'bundles' were formed during double-strand break repair (Lesterlin et al., 2014). These bundles are similar to RecA structures called 'threads', that nucleate at engineered double-strand breaks in *Bacillus subtilis* (Kidane and Graumann, 2005). RecA bundles form after SOS induction by other means than double-strand breaks, and also then interact with anionic phospholipids in the inner membrane (Garvey et al., 1985; Rajendram et al., 2015). The appearance of elongated RecA* foci after treatment with UV has not always been associated with bundle formation (Renzette et al., 2007). It should be noted that whereas assemblies of RecA observed *in vivo* have been variously referred to as filaments, threads or bundles, their correspondence to the *in vitro* observations of RecA aggregates referred to as 'rods' or 'bundles' remains unclear.

112 Due to the similar morphology of the fluorescence signal arising from these various DNA-
113 bound repair or DNA-free storage structures, teasing out dynamics of individual repair
114 complexes in live cells has proven difficult. The limited functionality of RecA fusion proteins
115 utilized to date also raises concerns about the relationship of the observed structures to
116 normal RecA function. Several fundamental questions remain unanswered: When and
117 where does SOS signaling occur in cells? How is excess RecA stored?

118 In this work, we describe the development of a probe that specifically visualizes RecA
119 structures on DNA, and utilize it as part of a broader effort to provide a detailed time line of
120 RecA structural organization in living cells after DNA damage. With the objective of
121 selectively localizing DNA-bound and ATP-activated RecA* as a key repair intermediate
122 inside living cells, we produced a monomeric, catalytically dead N-terminal truncation of the
123 bacteriophage λ repressor CI (mCI*; CI 101-229, A152T, P158T, K192A*) that retains the ability
124 to bind RecA-ssDNA filaments. Removal of the N-terminal domain renders the mCI unable to
125 bind DNA, leaving only RecA* as a binding partner. Using both untagged and fluorescently
126 labelled mCI constructs, we document the effects of mCI *in vitro* and *in vivo*. We use mCI as
127 well as the most functional RecA-GFP fusion protein variants to distinguish between the
128 various types of RecA structures and follow their behavior through time. In addition, we
129 examine the location of RecA* foci formed in the nucleoid in relation to the location of the
130 cellular replisomes. Our results reveal how the activity of RecA is regulated upon triggering
131 of the SOS pathway and identify the various states of RecA that are relevant throughout the
132 damage response.

133 **Results**

134 **RecA-GFP forms different types of aggregates in cells**

135 Damage in the template strand can result in the stalling or decoupling of replication, leading
136 to the accumulation of single-stranded DNA. This ssDNA provides a RecA nucleation site to
137 form RecA*, the structure that amplifies the cellular signal for genetic instability (Figure 1A).
138 In response to DNA damage, transcription of the SOS-inducible genes is up-regulated.
139 Because production of RecA occurs rapidly after damage, it is critical to observe live cells at
140 early time points with high temporal resolution after SOS induction.

141 With the objective of characterizing the spatial and temporal organization of RecA in cells
142 during SOS induction, we performed time-lapse imaging of individual *E. coli* cells
143 immobilized in flow cells using a variety of fluorescent probes (See SI for imaging methods).
144 This setup enabled us to monitor growing cells with nutrient flow at 30°C, while keeping the
145 cells in place to support long-term, time-lapse imaging of individual cells. A quartz window
146 in the flow cell enabled us to provide *in situ* UV irradiation with a defined dose (20 Jm^{-2}) at
147 the start of the experiment. Following this, we monitored fluorescence every 5 minutes over
148 the course of three hours by wide-field acquisition (Figure 1B). For this study we chose to
149 induce SOS with UV for two key reasons: first, UV light is a strong inducer of the SOS

150 response, and second, a pulse of UV light serves to synchronize the DNA damage response
151 in cells that are continuously replicating DNA without the need for additional
152 synchronization.

153 First, we set out to characterize the temporal activity of the *recA* promoter alone in wild-
154 type MG1655 cells in response to ultraviolet radiation. We imaged cells that express fast-
155 folding GFP from the *gfpmut2* gene placed under the *recA* promoter on a low-copy reporter
156 plasmid, with a maturation time of less than 5 minutes ('pRecAp-gfp' cells; strain# HG260)
157 (Kalir et al., 2001; Zaslaver et al., 2006). The copy number of this reporter plasmid has been
158 shown to remain unchanged in response to ultraviolet radiation (Ronen et al., 2002). The
159 cells retain the chromosomal copy of the wild type *recA* gene. Measurements of the mean
160 fluorescence intensity of cytosolic GFP in pRecAp-gfp cells exhibited a gradual increase
161 peaking at approximately 135 min, with a maximum that corresponded to a two-fold
162 increase compared to the initial fluorescence intensity (SI Movie 1 & Figure 1C). After UV
163 exposure, the accumulation of the fluorescent reporter protein expressed from the *recA*
164 promoter reaches a maximum only after more than two hours. By extension, this gradual
165 increase is used here to define the time period during which cellular RecA concentration is
166 increasing after UV treatment.

167 Next, we imaged MG1655 cells that carry a *recA-gfp* fusion allele expressed from the
168 *recAo1403* operator in place of the wild-type chromosomal copy of *recA* ('*recA-gfp*' cells;
169 strain# HG195). The *recAo1403* promoter increases the basal (non-SOS) level of *recA*
170 expression by a factor of 2-3 (Rajendram et al., 2015; Renzette et al., 2005). Despite the
171 higher expression level, cells expressing this RecA-GFP fusion protein are deficient in RecA
172 functions; notably, these cells exhibit a three-fold lower survival in response to UV
173 irradiation, and ten-fold lower ability to perform recombination (Renzette et al., 2005).
174 Additionally, these cells exhibit delayed kinetics of SOS induction, but are still able to induce
175 the SOS response to the same extent as wild-type cells (Renzette et al., 2005). In response
176 to UV irradiation, GFP fluorescence in *recA-gfp* cells increased after DNA damage and
177 peaked at approximately 130 min (SI Movie2 & Figure 1C & 1D). Thus, the kinetics of the
178 observed increase in the levels of chromosomally expressed RecA-GFP fusion protein are the
179 same those of the increase seen with the plasmid-based *gfpmut2* reporter under control of
180 the *recA* promoter.

181 Measurements of the abundance of the *recA* transcript after SOS induction have revealed a
182 ten-fold increase within minutes after irradiation with UV (Courcelle et al., 2001). In bulk
183 experiments, the amount of RecA protein has been shown to attain a maximum at 90 min
184 after introduction of damage (Salles and Paoletti, 1983). Results from our live-cell
185 experiments are generally consistent with these studies, revealing that the amount of RecA
186 accumulated in cells attains a maximum at a time after triggering the SOS response that is
187 much later than the de-repression of the *recA* promoter. During the SOS response, many
188 cells undergo filamentation as cell division is blocked while some DNA synthesis continues

189 (Howard-Flanders et al., 1968). The increase in gene expression counters the dilution in the
190 cellular RecA concentration that is caused by the filamentation of the cells.

191 In these experiments, RecA-GFP formed well-defined features both before and after DNA
192 damage (SI Movie 2 and Figure 1D). These foci exhibited various morphologies ranging from
193 punctate foci to bundles. The foci became generally larger and more abundant after UV
194 irradiation. To determine whether RecA foci formed in the absence of DNA damage are
195 functionally distinct from those formed during the SOS response, we set out to specifically
196 visualize RecA*, the complex that is formed when RecA binds ssDNA and that is actively
197 participating in repair. To that end, we investigated interaction partners of the ssDNA-RecA
198 filament that are not endogenously present in *E. coli*. Since the MG1655 strain we use in
199 our studies is cured of bacteriophage λ, we focused on co-opting the λ repressor to detect
200 RecA* in cells (Figure 1E) (Roberts and Roberts, 1975).

201 **The monomeric C-terminal fragment of the bacteriophage λ repressor (mCI) stabilizes**
202 **dynamics of RecA-ssDNA filaments *in vitro***

203 The bacteriophage λ repressor CI is responsible for the maintenance of lysogeny in *E. coli*
204 infected with phage λ (Echols and Green, 1971). Oligomers of CI bind the operator regions in
205 the constitutive P_L and P_R promoters in λ DNA and inhibit transcription from these
206 promoters (Ptashne et al., 1980). In response to DNA damage, the λ repressor CI exhibits
207 RecA* dependent auto-proteolysis, much like the homologous proteins in bacteria, LexA
208 and UmuD (Burckhardt et al., 1988; Ferentz et al., 1997; Luo et al., 2001; Roberts and
209 Roberts, 1975; Stayrook et al., 2008; Walker, 2001). In this reaction, the ssDNA-RecA
210 filament (RecA*) stabilizes a proteolysis-competent conformation of CI enabling auto-
211 proteolysis at Ala111-Gly112 (Ndjonka and Bell, 2006; Sauer et al., 1982). This co-protease
212 activity of the RecA* filament results in loss of lysogeny due to de-repression of
213 transcription of *cI* and prophage induction of λ. The N-terminal DNA-binding domain of CI is
214 dispensable for interactions with RecA*(Gimble and Sauer, 1989). A minimal C-terminal
215 fragment of the λ repressor CI(101-229 A152T P158T K192A) (henceforth referred to as mCI,
216 Molecular weight 14307.23 Da; Figure 1F) efficiently inhibits the auto-catalytic cleavage of a
217 hyper-cleavable monomeric C-terminal fragment CI(92-229) (Ndjonka and Bell, 2006). Cryo-
218 electron microscopy has revealed that the mCI binds deep in the groove of the RecA
219 filament (Galkin et al., 2009).

220 Given the existing extensive *in vitro* characterization of mCI, we decided to further develop
221 it as a probe for detecting RecA* in cells. To better understand the kinetics, cooperativity
222 and affinity of mCI for RecA-ssDNA filaments, we first pursued an *in vitro* investigation of the
223 interaction between mCI and RecA filaments. Additionally, to visualize mCI in live-cell
224 experiments, we made fusion constructs with fluorescent proteins tagged to the N terminus
225 of mCI via a 14-amino acid linker. To perform time-lapse imaging, we tagged mCI with the
226 yellow fluorescent protein YPet, and to perform live-cell photoactivatable light microscopy
227 (PALM), we tagged mCI with the photoactivatable red fluorescent protein PAmCherry.

228 Untagged mCI and the two fluorescently labelled constructs, PAmCherry-mCI and YPet-mCI
229 were purified and characterized for RecA-ssDNA binding as described below (See SI for
230 details, SI Figure 1A).

231 Binding of the mCI constructs to ssDNA-RecA filaments was first assayed by surface plasmon
232 resonance (SPR). We immobilized a 5' biotinylated $(dT)_{71}$ ssDNA substrate on the surface of
233 a streptavidin-functionalized SPR chip (Figure 2A) and assembled RecA-ssDNA filaments by
234 injecting 1 μM RecA in buffer supplemented with ATP. This was followed by injection of
235 buffer without RecA, but supplemented with ATPγS to minimize disassembly of the RecA
236 filament on the ssDNA immobilized on the chip surface (SI Figure 1B). Next, the experiment
237 was repeated but now introducing to pre-formed RecA* filaments solutions that not only
238 contain stabilizing ATPγS, but also either untagged or fluorescently tagged mCI proteins.
239 Figure 2B shows scaled sensorgrams that are corrected for any disassembly of the ssDNA-
240 RecA-ATPγS filament and thus reporting on interactions of mCI with the highly stable RecA*
241 filament (see also SI Figure 1C). These sensorgrams reveal that mCI associates with the RecA
242 filament in a biphasic manner. Dissociation of mCI from the RecA filament was slow, with a
243 dissociation halftime ($t_{1/2}$) of 850 s. In comparison, the fluorescently tagged constructs
244 dissociated faster, but still slowly enough for use as a probe for the detection of RecA*. We
245 measured a $t_{1/2}$ = 260 s and 280 s for YPet-mCI and PAmCherry-mCI respectively.

246 To probe the influence of mCI binding on the conformational state of the RecA* filament,
247 we next studied association of mCI with ssDNA-RecA-ATP filaments using single-molecule
248 Förster Resonance Energy Transfer (FRET) experiments. We used a previously described
249 DNA substrate consisting of a biotinylated 18-mer double-stranded region preceded by a 5'
250 $(dT)_{40}$ overhang ('bio-ds18-$(dT)_{40}$', See SI for details, Figure 2C) (Park et al., 2010). This
251 substrate represents the partly single-stranded and partly double-stranded nature of the
252 DNA substrate that is thought to be generated in the context of replisomes encountering
253 lesions *in vivo*. The ssDNA region is labelled with a Cy3 donor probe on one end and a Cy5
254 acceptor probe on the other so that the degree of extension of the ssDNA can be measured
255 by FRET. The DNA substrate was immobilized on a streptavidin-coated surface in a flow cell
256 and the Cy5 FRET signal was measured upon excitation of the Cy3 dye with a 532-nm laser
257 (see SI for details). Consistent with previous FRET investigations of this DNA substrate (Park
258 et al., 2010), the DNA substrate alone exhibited a FRET distribution with a mean value of
259 0.43 ± 0.07 (mean ± standard deviation of a single Gaussian fit to the data) reflecting the
260 ability of the ssDNA overhang to entropically collapse and sample a large number of
261 conformational states (Figure 2C, 2G & 2I; see 'DNA' trace). In the presence of ATP and
262 RecA, the resulting FRET distribution exhibited a peak with a mean FRET value of 0.3 ± 0.1,
263 consistent with the formation of a highly dynamic RecA filament undergoing simultaneous
264 assembly and disassembly (Figure 2D, 2G and 2I 'ATP' trace). Upon incubating the DNA
265 substrate with RecA in the presence of ATPγS, we observed a shift in the FRET distribution to
266 an even lower value of 0.2 ± 0.07, reflecting the formation of a rigid, fully extended ssDNA-
267 RecA filament (Figure 2E, 2G and 2I 'ATPγS'). Since ATPγS traps the RecA filament in an

268 'active' conformation that is capable of LexA repressor autocatalytic cleavage, we
269 interpreted the 0.2 FRET state as corresponding to the active state (Craig and Roberts,
270 1981). Incubation of RecA with ADP revealed a broad FRET distribution similar to that
271 obtained in the presence of ATP, reflecting unstable RecA filaments assembled on the DNA
272 overhang (See SI Figure 2A).

273 Next, we studied the FRET displayed by the ssDNA-RecA-ATP filament while titrating in
274 purified mCI (Figure 2H and SI Figure 2B) to gain insight into the influence of mCI binding on
275 the stability of ssDNA-RecA-ATP filaments (Figure 2F). In the presence of mCI the FRET
276 substrate exhibited a bi-modal behavior: either molecules exhibited the 0.43 FRET state or
277 the 0.2 FRET state. Upon increasing mCI concentration, the FRET distribution gradually
278 shifted from a mean of 0.43 to 0.2 in response to higher concentrations of mCI (Figure 2H).
279 By fitting the distributions to a sum of two Gaussian fits reflecting the 'bound' state (0.2
280 FRET) and 'unbound' state (0.4 FRET), we were able to obtain the bound fraction at every
281 concentration of mCI tested (Figure 2H and 2J). Fitting these data to the Hill equation
282 yielded an equilibrium dissociation constant of 36 ± 10 nM with a Hill coefficient of 2.4 ± 0.2
283 (Figure 2J). The increase in the population of molecules in the lowest FRET state in response
284 to an increase in mCI concentration demonstrates that mCI stabilizes the RecA filament in
285 the active conformation.

286 Examination of the FRET traces revealed that in the presence of mCI, the DNA substrate
287 exhibits stochastic transitions from the RecA-bound to the unbound state (e.g., Figure 2I for
288 [mCI] = 10 nM). The frequency of these transitions to the unbound state decreased in the
289 presence of high concentration of mCI (Figure 2I, see also SI Figure 2B). FRET traces of DNA
290 substrates in the presence of RecA and saturating concentrations of mCI (3 μM) exhibited
291 stable, long-lived binding events at a FRET value of 0.2 over the time scale of acquisition
292 (Figure 2G). To obtain off rates from the data, we applied a threshold of 0.3 (SI Figure 2C) to
293 segment the trajectories such that segments with FRET values less than 0.3 were considered
294 to reflect the 'bound' state, and those above 0.3 were considered to be the 'unbound' state.
295 The cumulative residence time distributions for the binding events (low FRET values) in the
296 FRET trajectories were best fit by a sum of two exponentials decaying according to a fast off
297 rate $k_{off,1}$ = 0.23 ± 0.06 s^{-1} and a slow off rate $k_{off,2}$ = 0.044 ± 0.002 s^{-1} (Figure 2K). These off-
298 rates were largely independent of the concentration of mCI (Figure 2K). However, strikingly,
299 the fraction of the population decaying following the slower off rate increased from 35% in
300 the absence of mCI to 91% in the presence of 1μM mCI (Figure2L).

301 Next we probed the influence of mCI on the ability of RecA* to perform three key catalytic
302 functions *in vitro*: LexA cleavage, ATP hydrolysis and strand-exchange. Incubation of pre-
303 formed RecA* filaments on circular ssDNA M13mp18 substrates with micromolar
304 concentrations of mCI revealed a pronounced inhibition of RecA* ATPase activity (SI Figure
305 2D). The tagged mCI variants did not significantly inhibit RecA* ATPase activity at
306 concentrations under 500 nM (SI Figure 2D). Monitoring of LexA cleavage by RecA* in the

307 presence of mCI revealed that even high concentrations of mCI did not inhibit LexA
308 cleavage, at best, mCI at micromolar concentrations slowed the kinetics of LexA cleavage
309 (Supplementary Fig. 2E). Finally, whereas strand-exchange by RecA* was potently inhibited
310 at micromolar concentrations of mCI (Supplementary Fig. 2F), tagged mCI constructs did not
311 significantly inhibit strand-exchange activity at concentrations below 500 nM
312 (Supplementary Fig. 2F).

313 Taken together, these *in vitro* investigations provide insights into the consequences of mCI
314 binding on the activity of RecA*. We found that mCI stabilizes the RecA* filament in the
315 'active' conformation that is capable of LexA cleavage. At high concentrations (5 – 10 μM),
316 mCI can inhibit ATP hydrolysis and strand-exchange by RecA*, and delay LexA cleavage. This
317 is consistent with mCI binding to the RecA nucleoprotein filament groove as anticipated.
318 Importantly, at low concentrations (10 - 100 nM) similar to those we eventually employed
319 as a standard in vivo (as described below), these key activities of RecA* are not significantly
320 affected by the presence of mCI or tagged variant. These findings emphasize the suitability
321 of the use of mCI derived probes for probing RecA* function.

322 **mCI inhibits SOS induction in a concentration-dependent manner**

323 We probed whether mCI interacts with ssDNA-RecA filaments (RecA*) in cells upon DNA
324 damage and potentially inhibits the SOS response. To that end, we created live-cell imaging
325 vectors that express either mCI or the PAmCherry-mCI fusion from the *araBAD* promoter in
326 a tunable manner depending on the amount of L-arabinose provided in the growth medium
327 (Guzman et al., 1995). The ability of cells to induce SOS was assayed using a previously
328 described set of SOS-reporter plasmids that express GFP in response to DNA damage
329 (Zaslaver et al., 2006). In this assay, we measured the fluorescence of fast-folding GFP
330 expressed from the *gfpmut2* gene under the SOS-inducible *sulA* promoter on a low-copy
331 plasmid ('*sulAp-gfp*')(Zaslaver et al., 2006). As a control, we also measured GFP fluorescence
332 from the promoter-less parent vector ('*gfp*'). The copy number of these SOS-reporter
333 plasmids is not influenced by the ultraviolet radiation (Ronen et al., 2002). To measure the
334 ability of mCI to inhibit the SOS response in cells, we co-transformed wild-type MG1655 cells
335 with either the pBAD-mCI vector ('*mcI*'), pBAD-PAmCherry-mCI vector ('*PAmCherry-mcI*') or
336 an empty pBAD vector ('pBAD'), and *sulA* reporter ('*sulAp-gfp*') or promoter-less vector
337 ('*gfp*') to generate four strains: 1. cells that carry the empty pBAD vector and the promoter-
338 less *gfp* vector ('*gfp*+pBAD', strain# HG257) 2. cells that carry the empty pBAD vector and
339 the *sulA* reporter plasmid ('*sulAp-gfp* + pBAD', strain# HG258) 3. cells that carry the pBAD-
340 mCI vector and the *sulA* reporter plasmid ('*sulAp-gfp* + *mcI*', strain# HG253) and 4. cells that
341 carry the pBAD-PAmCherry-mCI vector and the SOS-reporter plasmid ('*sulAp-gfp* +
342 *PAmCherry-mcI*', strain# HG285).

343 We then acquired time-lapse movies of these cells to observe the evolution of the SOS
344 response over three hours after UV damage (Figure 3A). As expected, when cells carrying
345 the *sulA* reporter plasmid and the empty pBAD vector ('*sulAp-gfp* + pBAD') were irradiated

346 with a 20 Jm^{-2} dose of UV, we observed a robust increase in GFP fluorescence (Figure 3A;
347 strain# HG258). In contrast, cells carrying the promoter-less control vector and the empty
348 pBAD vector ('*gfp*+pBAD') vectors did not exhibit any increase in GFP fluorescence in
349 response to UV (Figure 3A, summarized in Figure 3C; strain# HG257).

350 After these experiments confirming the robustness of the *sulA* reporter as a readout for SOS
351 induction, we grew cells carrying both the *sulA* reporter and the mCI vectors ('*sulAp-gfp* +
352 *mcI*', strain# HG253) in imaging medium containing 0, 10^{-3} or 10^{-2} % L-arabinose and
353 immobilized them in flow cells. In this L-arabinose concentration regime, we expect the mCI
354 copy number to be approximately 20, 50 and 500 copies per cell, respectively (Ghodke et al.,
355 2016). Time-lapse acquisition after UV irradiation revealed that SOS induction was sensitive
356 to the presence of mCI. Even leaky expression of mCI caused a measurable delay in GFP
357 fluorescence (Figure 3A). This delay was found to be proportional to the expression level of
358 mCI, and cells grown in 10^{-2} % L-arabinose exhibited nearly complete inhibition of SOS
359 induction during the experimental timeline of three hours after UV irradiation (Figure 3A
360 and 3C). Time-lapsed imaging of wild-type cells carrying the pBAD-PAmCherry-mCI vector
361 and the *sulA* reporter plasmid ('*sulAp-gfp* + *PAmCherry-mcI*', strain# HG285) also revealed a
362 similar delay in SOS induction depending on the concentration of L-arabinose in the growth
363 medium (Figure 3B). These data suggest that mCI competes with LexA in cells at sites of
364 RecA* in response to DNA damage.

365

366 **Most RecA filaments are formed at sites distal to replisomes after DNA damage**

367 A long-standing model for SOS induction predicts that RecA* filaments are formed on
368 chromosomal DNA when replisomes encounter UV lesions (Sassanfar and Roberts, 1990).
369 These RecA* filaments are believed to be the sites of SOS induction. While several lines of
370 evidence support the model that RecA* filaments are formed after UV irradiation, direct
371 visualization in living *E. coli* cells has not been demonstrated. Given that mCI robustly
372 interacts with RecA* filaments, we set out to visualize RecA* in cells exposed to UV light.
373 Importantly, considering that mCI can inhibit RecA* activities at µM concentrations, we
374 chose to express mCI variants from the tightly repressed, and tunable pBAD promoter.
375 Incubating cells with low concentrations of L-arabinose results in cells expressing tagged
376 mCI constructs in the 10-100 nM range in cells.

377 This was achieved by imaging a two-color strain that expresses a chromosomal YPet fusion
378 of the *dnaQ* gene (that encodes the replisomal protein ε, a subunit of the replicative DNA
379 polymerase III), and PAmCherry-mCI from the pBAD-PAmCherry-mCI plasmid in the
380 presence of L-arabinose (strain# HG267). The YPet fusion has previously been shown to
381 minimally affect the function of ε (Reyes-Lamothe et al., 2010; Robinson et al., 2015). The
382 two-color strain was grown in medium containing small amounts of L-arabinose ($5x10^{-4}$ %)
383 to induce low expression of PAmCherry-mCI. Under these conditions, UV-surivival of HG267

384 was indistinguishable from that of MG1655/pBAD-mycHisB(strain# HG116) (SI Figure
385 3A).This was followed by time-lapse imaging (5 min intervals for 3 h after 20 Jm^{-2} of UV) in
386 flow-cells. In this experiment, we performed live-cell PALM to detect PAmCherry-mCI, and
387 TIRF imaging to detect replisomes (see SI for technical details related to imaging, SI Figure
388 3B). This approach enabled us to visualize replisomes as well as mCI foci (Figure 4A). To
389 compare cells in the presence and absence of SOS induction, we carried out the same
390 experiments in cells carrying the *lexA3*(Ind^-) allele (strain# HG311; Figure 3C). These cells
391 express a non-cleavable mutant of the LexA repressor (G85D) that binds RecA*, but fails to
392 induce SOS (Figure 4A and B) (Markham et al., 1981).

393 SOS induction resulted in an increase in mCI/RecA foci. In the absence of DNA damage, 19%
394 of all *lexA*$^+$ cells exhibited at least one PAmCherry-mCI focus (Figure 4A and 4C (green line), *t*
395 = -5 min; summarized in Figure 4H). In response to UV damage inflicted at *t* = 0 min, we
396 detected an increase in the number of *lexA*$^+$ cells with at least one PAmCherry focus to 56%
397 of the population at *t* = 60 min after UV (green line, Figure 4C, total numbers for each time
398 point are presented in SI Figure 3C). The number of replisome foci detected per cell was
399 found to remain relatively constant ranging from 3.5 ± 0.14 (mean ± standard error) in the
400 absence of UV to 4.2 ± 0.2 per cell at *t* = 60 min after UV (blue line, Figure 4D). The number
401 of PAmCherry-mCI foci marking sites of RecA* was found to increase approximately five-fold
402 from 0.3 ± 0.15 per cell before UV irradiation to 1.4 ± 0.25 per cell at *t* = 60 min (red line,
403 Figure 4D). Among cells exhibiting at least one focus, 24 ± 8% (mean ± standard error) of
404 PAmCherry-mCI foci co-localized with replisomes before UV irradiation, and this number
405 increased to 34 ± 5% at 60 min after UV (Figure 4F and 4I).

406 Blocking SOS induction also limited RecA/mCI focus formation. Only 1.5% of the *lexA3*(Ind^-)
407 (gray line Figure 4C) population exhibited at least one PAmCherry-mCI focus (compared to
408 19% for wild-type) (summarized in Figure 4H) in the absence of UV. Additionally, the
409 number of PAmCherry-mCI foci detected remained consistently low, with 0.28 ± 0.17 foci
410 per cell compared to *lexA*$^+$ cells (compare red lines in Figure 4E and 4D), suggesting that the
411 inability to cleave LexA results in an absence of available binding sites for PAmCherry-mCI.
412 Strikingly, *lexA3*(Ind^-) cells did not exhibit PAmCherry-mCI foci that co-localized with
413 replisomes before UV irradiation (Figure 4G). At 60 minutes after UV irradiation, only 21% of
414 the population exhibited PAmCherry-mCI foci compared to 56% in case of the wild-type
415 (Figure 4C, 4H). Of these, 32 ± 11% of the PAmCherry-mCI foci co-localized with replisomes
416 at 60 minutes (Figure 4G, 4I). These results are consistent with the model that some RecA*
417 filaments are formed in cells in the vicinity of replisomes when cells are exposed to UV light.
418 Most RecA* filaments are formed at locations distal to the replisome.

419 14 ± 5% of the replisomes exhibited co-localization with mCI in *lexA*$^+$ cells exhibiting
420 PAmCherry-mCI foci (Figure 4F). These results suggest that in approximately twenty percent
421 of the population RecA filaments are formed during normal growth (Figure 4C, 'No UV' time
422 point). However only approximately 24% of these are associated with replisomes (blue line,

423 Figure 4F, 'No UV' time point). These RecA* filaments formed at sites of replisomes in the
424 absence of UV light might reflect replication forks engaged in recombination-dependent
425 DNA restart pathways or replication forks stalled at sites of bulky endogenous DNA damage.
426 In contrast, fewer *lexA3*(Ind$^-$) cells exhibited PAmCherry-mCI foci suggesting that the non-
427 cleavable LexA(G85D) protein competes with mCI for the same substrates *in vivo*. These
428 results reinforce our observations that mCI and LexA compete for the same binding
429 substrates *in vivo*.

430 **RecA forms bundles that are stained by mCI in cells**

431 Previous studies have noted the formation of large macromolecular assemblies of RecA in
432 response to double-strand breaks in cells (Lesterlin et al., 2014). These aggregates of RecA-
433 GFP have been termed 'bundles' (Figure 1C and references (Lesterlin et al., 2014; Rajendram
434 et al., 2015)). Our experiments with MG1655/pBAD-PAmCherry-mcI also revealed
435 localizations of mCI that resembled RecA bundles (Figure 5A). These observations were also
436 reproduced in cells expressing YPet-mCI from a pBAD plasmid (strain# HG143). Cells were
437 induced with 10^{-3} % L-arabinose, immobilized in flow cells, irradiated with a dose of 20 Jm^{-2}
438 of UV, and imaged using a time-lapse acquisition protocol. In this experiment, YPet-mCI
439 initially exhibits cytosolic localization at the start of the experiment (Figure 5B, t = -5 min
440 ('No UV' time point)) and reveals foci and bundles at later time points (Figure 5B, t = 1 h and
441 2 h).

442 Next, we tested whether the formation of these bundles required RecA that has wild-type
443 functions. To that end, we imaged YPet-mCI in DH5α cells that carry the *recA1* allele (an
444 inactive mutant, G160D) (Bryant, 1988). These cells did not exhibit foci or bundles that
445 bound to YPet-mCI after UV (Figure 5C, strain# HG242). These data demonstrate that mCI
446 recognizes a specific configuration of wild-type RecA on ssDNA – one that is able to co-
447 operatively bind and hydrolyze ATP.

448 The UvrD helicase performs a critical role in disassembling RecA filaments in cells (Centore
449 and Sandler, 2007; Lestini and Michel, 2007; Petrova et al., 2015; Veaute et al., 2005). Since
450 mCI stabilizes RecA-ssDNA filaments *in vitro*, we hypothesized that persistent RecA*
451 filaments would lead to constitutive SOS in Δ*uvrD* cells lacking the ability to disassemble
452 RecA*. To test this hypothesis, we imaged Δ*uvrD* cells (strain# HG235) expressing plasmid-
453 based YPet-mCI and found that these cells indeed exhibited constitutive RecA bundles. The
454 presence of constitutive SOS in these cells is further confirmed by the observation of a
455 strong filamentation, even in the absence of any external DNA damage (SI Figure 4).

456 Taken together, these results demonstrate that: 1) RecA bundles are not only formed by
457 RecA-GFP but also by wild-type RecA during the SOS response and 2) The ability to form a
458 high-affinity complex on ssDNA is critical for the formation of RecA bundles. Further, the
459 lack of mCI features in the *recA1* background suggest that far from being DNA-free

460 aggregates of RecA, these bundles contain an ordered assembly of RecA that is bound to
461 DNA.

462 **RecA forms storage structures that are not stained by mCI**

463 We then turned our attention to focus on how RecA is stored in cells. Storage structures of
464 RecA would need to satisfy two criteria to be distinguished from complexes active in DNA
465 repair and from polar aggregates representing mis-folded proteins: 1) the size or number of
466 these structures should be proportional to the amount of RecA present in the cell and 2)
467 RecA stored in these structures should be available for biological function when required,
468 that is, after DNA damage. To detect storage structures of RecA in live cells, we imaged
469 *recA-gfp* cells in the absence of DNA damage (strain# HG195). Cells exhibited punctate foci
470 that appear to be positioned outside the nucleoid (Figure 6A). Since the cells did not exhibit
471 additional markers of distress, namely cell filamentation, we presumed that the RecA
472 features correspond to storage structures of RecA. We hypothesized that the size of these
473 punctate foci is dependent on the copy number of RecA in cells. To test this hypothesis, we
474 pursued a strategy involving over-expression of unlabeled RecA from a plasmid in *recA-gfp*
475 cells and measuring whether the foci become larger as the amount of untagged RecA
476 increases and integrates into the structures with the labelled RecA.

477 To that end, we created plasmids that expressed wild type RecA protein at two different
478 levels. First, a low-copy plasmid expressed *recA* from the constitutive *recAo281* operator
479 (pConst-RecA; see SI for details) (Uhlin et al., 1982; Volkert et al., 1976). A second version of
480 that plasmid (pG353C-RecA) cut expression in half by incorporating an altered ribosome
481 binding site (RBS) (see SI Figure 5A). We then imaged *recA-gfp* cells carrying one or the
482 other of these plasmids. Time-lapsed imaging of undamaged cells (5 min intervals for 3h)
483 revealed that the RecA-GFP signal was confined to a single large feature (Figure 6A). To
484 quantify the size of RecA features in the absence of DNA damage, we measured the
485 maximum Feret diameter (referring to the largest physical dimension of the structure;
486 Figure 6A) of the feature at a threshold above the background (Figure 6B, see SI for details).
487 Comparison of the Feret diameters of features in *recA-gfp* cells carrying the pConst-RecA
488 and pG353C-RecA vectors revealed a strong dependence on the expression level of
489 untagged wild-type RecA protein (Figure 6B). *recA-gfp*/pConst-RecA cells exhibited larger
490 features than *recA-gfp*/pG353C-RecA cells or *recA-gfp* cells alone. Notably, the storage
491 structures exhibited cross-sections that were circular (in the case of *recA-gfp cells)* or
492 elliptical (in the case of *recA*-gfp/pConst-RecA or *recA-gfp/*pG353C-RecA cells) unlike the
493 previously described thread-like filamentous RecA-bundles (Kidane and Graumann, 2005;
494 Lesterlin et al., 2014). In the absence of DNA damage, these structures were stably
495 maintained in cells in *recA-gfp*/pG353c-RecA cells (SI movie 3). Upon cell division, these
496 structures were disproportionately inherited by daughter cells. Notably, cells did not exhibit
497 markers of distress consistent with induction of SOS, suggesting that these storage
498 structures do not impede DNA replication during growth, and are likely not assembled on

499 DNA. Since the presence and size of these features is dependent on the amount of RecA
500 present in cells, henceforth we refer to them as a 'storage structures'.

501 To exclude the possibility that RecA-GFP storage structures are artefacts of the GFP fusion,
502 we collected electron-microscopy images of immunogold-stained RecA in four genetic
503 backgrounds: 1) Δ*recA*; 2) wild-type MG1655; 3) MG1655/pConst-RecA; and 4) *recA-*
504 *gfp*/pConst-RecA (Figure 6 panels C-F, respectively). As expected, clusters of gold-labelled
505 RecA antibodies could be observed in all samples except Δ*recA* cells (Figure 6C). Cells
506 carrying the over-expresser plasmid pConst-RecA exhibited strong RecA staining that was
507 localized to the membrane (Figure 6E, 6F. See SI Figure 5B for additional examples). These
508 results support the conclusion that excess RecA is stored in the form of membrane-
509 associated, storage structures even in cells carrying untagged, wild-type RecA.

510 Stored RecA should be made available to support repair during the SOS response. We tested
511 this hypothesis by exposing *recA-gfp*/pG353C-RecA cells to ultraviolet radiation and
512 monitoring the dynamics of the storage structures in time-lapsed fashion. We found that
513 the storage structures dissolve within one hour after introducing damage, flooding the cell
514 with RecA-GFP (Figure 6G, t = 1 h). At later time points, the storage structures re-appeared
515 at locations close to the poles (Figure 6G, t = 2 h 45), suggesting that the RecA is stored
516 away until needed (see also SI Movie 4). We characterized the dynamics of storage structure
517 disassembly by plotting the cumulative probability of loss of storage structures for the
518 population of cells that possessed a distinct storage structure as a function of time (Figure
519 6H; orange curve). We found that for *recA-gfp*/pG353C-RecA cells, half of the storage
520 structures were lost within 45 $\pm$ 5 min after UV damage (see SI for details). We then plotted
521 the cumulative probability distribution of time of appearance of storage structures after SOS
522 induction (Figure 6H, green curve). In these cells, half of the population of storage structures
523 that formed after UV damage, did so after 135 $\pm$ 5 minutes after UV.

524 Next, we investigated whether mCI interacts with these storage structures. Fluorescence
525 imaging of plasmid-based YPet-mCI expressed from the pBAD promoter in wild-type cells
526 expressing pG353C-RecA (strain# HG446) did not reveal any morphological features
527 consistent with those of the storage structures observed in *recA-gfp*/pG353C-RecA cells.
528 YPet-mCI was found to be cytosolic in the absence of DNA damage, suggesting a lack of
529 stable association with RecA storage structures (Figure 6I, 'No UV' time point). As noted
530 earlier, foci were rare. As described before, in response to UV irradiation, cytosolic YPet-mCI
531 was found to form foci and bundles (Figure 6I, 120 min time point; see also SI Movie 4).
532 These results suggested that YPet-mCI does not interact with RecA storage structures.
533 Observations of cells expressing plasmid-based mCI in *recA-gfp*/pG353C-RecA revealed no
534 detectable influence of mCI on the morphology of these structures (SI Figure 5C), reinforcing
535 the interpretation that mCI does not interact with storage structures of RecA in the absence
536 of damage.

537 To further confirm that storage structures are indeed distinct from RecA bundles, we
538 characterized the kinetics of RecA-GFP bundle formation in *recA-gfp* cells (strain# HG195). In
539 these cells, RecA storage structures are small (Figure 6A) and indistinguishable from repair
540 foci. Upon UV irradiation, cytosolic RecA-GFP forms foci that progress to form large, cell-
541 spanning bundles over the course of several tens of minutes (see SI Movie2), unlike RecA
542 storage structures observed in the *recA-gfp*/pG353C-RecA cells. Plotting a cumulative
543 probability distribution of time of incidence of bundle formation revealed that half of all
544 bundles in *recA-gfp* cells appear by 60 minutes after UV (Figure 6H, red curve). This timing is
545 consistent with measurements of incidence of bundle formation during double-strand break
546 repair (Lesterlin et al., 2014).

547 **DinI promotes the formation of storage structures in cells**

548 The DinI protein is a modulator of RecA function (Lusetti et al., 2004a; Lusetti et al., 2004b;
549 Renzette et al., 2007). In solution, the C-terminal tail of DinI mimics ssDNA, enabling
550 interactions with monomeric RecA (Ramirez et al., 2000). Since free RecA assembles to
551 form storage structures, we next investigated whether storage of RecA was influenced by
552 DinI. Considering that expression level of RecA influences storage structure formation, we
553 first constructed a strain carrying the *recA-gfp* chromosomal fusion under its native wild-
554 type promoter (P_{wt}-*recA-gfp*; strain# EAW428). We deleted *dinI* in this background (strain#
555 EAW767). In the absence of DNA damage, we detected storage structures in fewer Δ*dinI*
556 cells (27% of 702 cells) compared to *dinI*$^{+}$ cells (43% of 855 cells). Additionally, these
557 structures were smaller (see Figure 6J). Over-expression of DinI from pBAD-DinI in Δ*dinI* cells
558 further confirmed this result: cells recovered storage structures in the presence of L-
559 arabinose (see SI Figure 5D). These findings suggest that RecA storage structure formation
560 may be promoted by DinI.

561 **Discussion**

562 In this work, we have used the C-terminal fragment of the λ repressor in conjunction with
563 single-molecule imaging techniques in live cells to examine RecA protein dynamics in
564 response to SOS induction. In the absence of DNA damage, we see that RecA is largely
565 sequestered in storage structures. Upon UV irradiation, these storage structures dissolve
566 and the cytosolic pool of RecA rapidly nucleates to form early SOS signaling complexes,
567 followed by RecA bundle formation at later time points. Our analysis indicates that the
568 bundles are bound to DNA and may be single extended RecA nucleoprotein filaments. Upon
569 completion of repair, RecA storage structures reform. Our use of the mCI reagent, which
570 associates with DNA-bound and activated RecA* complexes, allows us to eliminate the
571 ambiguity associated with earlier observations utilizing RecA fusion proteins with limited
572 functionality and for the first time provide access to the spatial and temporal behavior of
573 the various forms of RecA structures within the cell. In addition, whereas some RecA foci
574 that form after DNA damage co-localize with replisomes, the majority do not.

575 We set out to use binding partners of RecA to probe intracellular localization of SOS-
576 signaling RecA complexes. Several proteins associated with the SOS response, notably LexA,
577 UmuD, and the λ repressor, interact with RecA* to effect autocatalytic cleavage. The
578 interaction of these proteins with the activated RecA nucleoprotein filament has been a
579 subject of intense investigation (Cohen et al., 1981; Gimble and Sauer, 1985; Little, 1982).
580 Even though each of these proteins interacts with a different set of residues on the RecA*
581 filament, they all occupy the helical groove of the RecA filament prior to auto-proteolysis
582 (Frank et al., 2000; Galkin et al., 2009; Yu and Egelman, 1993). We sought to exploit this key
583 feature by using a fluorescently labelled C-terminal fragment of λ repressor CI (denoted
584 mCI) to visualize RecA-DNA complexes. The mCI construct binds specifically to RecA* (Figure
585 2, SI Figure1). Binding of mCI stabilizes RecA* in the 'active' conformation capable of
586 mediating transcription-factor cleavage, exhibiting an equilibrium dissociation constant of
587 36 ± 10 nM and a Hill coefficient of 2.4 ± 0.2 for the binding of mCI to ssDNA-RecA filaments
588 assembled on a dT_{40} ssDNA overhang. Based on previous findings that one mCI contacts two
589 RecA monomers, we estimate that up to six mCI molecules can decorate the RecA-ssDNA
590 filament composed of up to 13 RecA monomers on the dT_{40} DNA substrate under conditions
591 of saturating mCI concentration (Galkin et al., 2009; Ndjonka and Bell, 2006). The non-
592 cleavable mCI thus can decorate RecA filaments assembled on DNA. We confirmed that mCI
593 interacts with RecA filaments in live cells by probing SOS induction after UV damage (Figure
594 3). We found that mCI has the potential to robustly inhibit SOS induction at high
595 concentrations. SOS induction is retained, albeit delayed, at mCI concentrations employed
596 in this study.

597 The leading model for SOS induction is that replication forks fail at sites of lesions and
598 produce large tracts of ssDNA that templates nucleation of RecA filaments. Visualizing this
599 model in cells has been challenging due to the difficulties associated with co-localization of a
600 high-abundance protein (RecA) with a handful of replisomes. Our strategy involving
601 fluorescently tagged mCI enabled us to examine the location of RecA* foci in nucleoids
602 relative to the replisomes for the first time in *E coli*. We found that the average number of
603 replisome foci did not change after DNA damage, confirming that most replisomes are not
604 disassembled after UV (Figure 4). Live-cell PALM imaging of mCI revealed foci that depended
605 on the presence of wild-type RecA and DNA damage. Surprisingly, 20% of wild-type cells
606 exhibited RecA* foci during normal growth. However, only 24% of these co-localized with
607 replisomes. The remaining 76% of sites of RecA* detected during normal growth did not co-
608 localize with replisomes. Upon exposure to ultraviolet light, 56% of cells exhibited RecA*
609 foci that were visualized by mCI, with up to 35% of the RecA* foci co-localized with
610 replisomes at 60 min in rich media (Figure 4). A previous report on co-localization of RecA-
611 GFP with DnaX-mCherry in *Bacillus subtilis* growing in minimal media reported a basal co-
612 localization of 74.8 ± 8.4 % with an increase to 84.3 ± 5.8 % at 5 min after 40 Jm^{-2} UV
613 treatment (Lenhart et al., 2014). The extent of co-localization of RecA* and replisomes
614 detected in our experiments, in *E coli* cells growing in media that supports multi-fork

615 replication is lower both before and after UV irradiation. The RecA* foci that co-localize with
616 replisomes are likely associated with replisomes that are stalled at sites of DNA damage. We
617 postulate that RecA* foci that are not co-localizing with replisomes are forming in DNA gaps
618 that are formed and left behind by the replisome (Howard-Flanders et al., 1968; Rupp and
619 Howard-Flanders, 1968; Yeeles and Marians, 2013). Notably, most foci of the translesion
620 DNA polymerases IV and V also form at nucleoid locations that are distal from replisomes,
621 both before and after SOS induction (Henrikus et al., 2018; Robinson et al., 2015).

622 The large cell-spanning structures termed RecA threads or bundles (we have adopted the
623 latter term) (Kidane and Graumann, 2005; Lesterlin et al., 2014; Rajendram et al., 2015) that
624 form after SOS induction deserve special mention. Following the initial phase of RecA*
625 formation, cells expressing YPet-mCI, PAmCherry-mCI or RecA-GFP exhibited large RecA
626 bundles. The formation of these bundles was also contingent upon the presence of wild-
627 type RecA. The *recA1* allele in DH5α failed to support focus or bundle formation, consistent
628 with the inability of the RecA(G160D) in DH5α to induce SOS and HR functions (Bryant,
629 1988). Additionally, cells lacking UvrD exhibited constitutive RecA bundles. These bundles
630 are thus a hallmark of the DNA damage response and may have special functionality in the
631 homology search required for recombinational DNA repair (Lesterlin et al., 2014). Here, we
632 show that the bundles bind to our mCI probe. This implies that the bundles are either bound
633 to DNA and thus activated as RecA*, or at a minimum are in a RecA*-like conformation that
634 permits mCI binding. Interestingly, despite the differences in the nature of the DNA damage
635 inflicted, the timing of RecA bundle formation in our UV experiments coincided closely with
636 that of RecA bundles observed upon induction of site specific double-strand breaks in the
637 chromosome (Lesterlin et al., 2014). The bundles may thus be nucleated by RecA binding to
638 either gaps or resected double strand breaks. At later time points, polymerization of RecA
639 filaments nucleated at ssDNA gaps could extend onto dsDNA, and manifest as bundles in our
640 experiments. RecA bundles also interact with anionic phospholipids in the inner membrane
641 (Rajendram et al., 2015). Notably, UmuC also localizes primarily at the inner-membrane
642 upon production and access to the nucleoid is regulated by the RecA* mediated UmuD
643 cleavage (Robinson et al., 2015). This transition occurs late in the SOS response (after 90
644 min), at a time-point when most, if not all of the cells in the population exhibit RecA
645 bundles. The origins, maturation and additional catalytic roles of RecA bundles in the SOS
646 response require additional investigation.

647 Our experiments enable us to distinguish storage structures from SOS signaling complexes
648 and RecA bundles based on three qualities: 1. storage structures dissolve after UV damage
649 whereas RecA bundles are formed in response to DNA damage. 2. storage structures often
650 exhibit a polar localization, whereas RecA-bundles form along the cell length. 3. the SOS
651 signaling complexes and RecA bundles are visualized by binding to mCI, whereas the RecA
652 storage structures are not. Finally, we found that DinI promotes storage structure
653 formation: cytosolic RecA in normal growing cells was found to be sequestered in structures
654 by simply over-expressing DinI from a plasmid.

655 Taken together, these data for the first time provide a full picture of a process that was first
656 hypothesized by Story and co-workers in 1992 suggesting that RecA can undergo a phase
657 transition to form DNA-free assemblies in live cells and redistribute into the cytosol where it
658 becomes available for DNA-repair functions (Figure 7). Within a few minutes after
659 encountering bulky lesions, replication forks synthesize ssDNA substrates that are rapidly
660 coated by cytosolic RecA to form RecA*. These RecA* enable auto-proteolysis of LexA to
661 initiate the SOS response and increase the levels of cellular RecA protein. Meanwhile,
662 storage structures of RecA dissolve, making RecA available for biological functions. The
663 RecA* foci elongate over several hours into elaborate bundles that may have multiple
664 functions. Finally, excess RecA is sequestered away into storage structures approximately
665 two hours after DNA damage, after DNA repair is complete and normal growth is restored.

666 **Author contributions**

667 Conceptualization: H.G, M.M.C, and A.M.V.O.; Methodology: H.G. and A.M.V.O.; Formal
668 Analysis and Software: H.G. and B.P., Investigation, H.G., B.P., J.L. S.J. and R.W.; Writing –
669 Original Draft: H.G.; Writing – Review & Editing: H.G., M.M.C., R.W., and A.M.V.O.; Funding
670 Acquisition: A.M.V.O.; Resources: E.A.W., R.W.; Supervision: A.M.V.O.

671 **Acknowledgements**

672 We thank Douglas Weibel for the MG1655 RecA-GFP strain. We thank the Alon lab for the
673 SOS-reporter plasmids. We thank Amy McGrath and Celine Kelso for technical assistance
674 with ESI-MS analyses of purified proteins. R.W. was supported by the NICHD/NIH Intramural
675 Research Program. M.M.C is supported by NIH Grant GM32335. A.M.V.O. acknowledges
676 support by the Australian Research Council (DP150100956 and FL140100027).

677

678 **Figure legends**

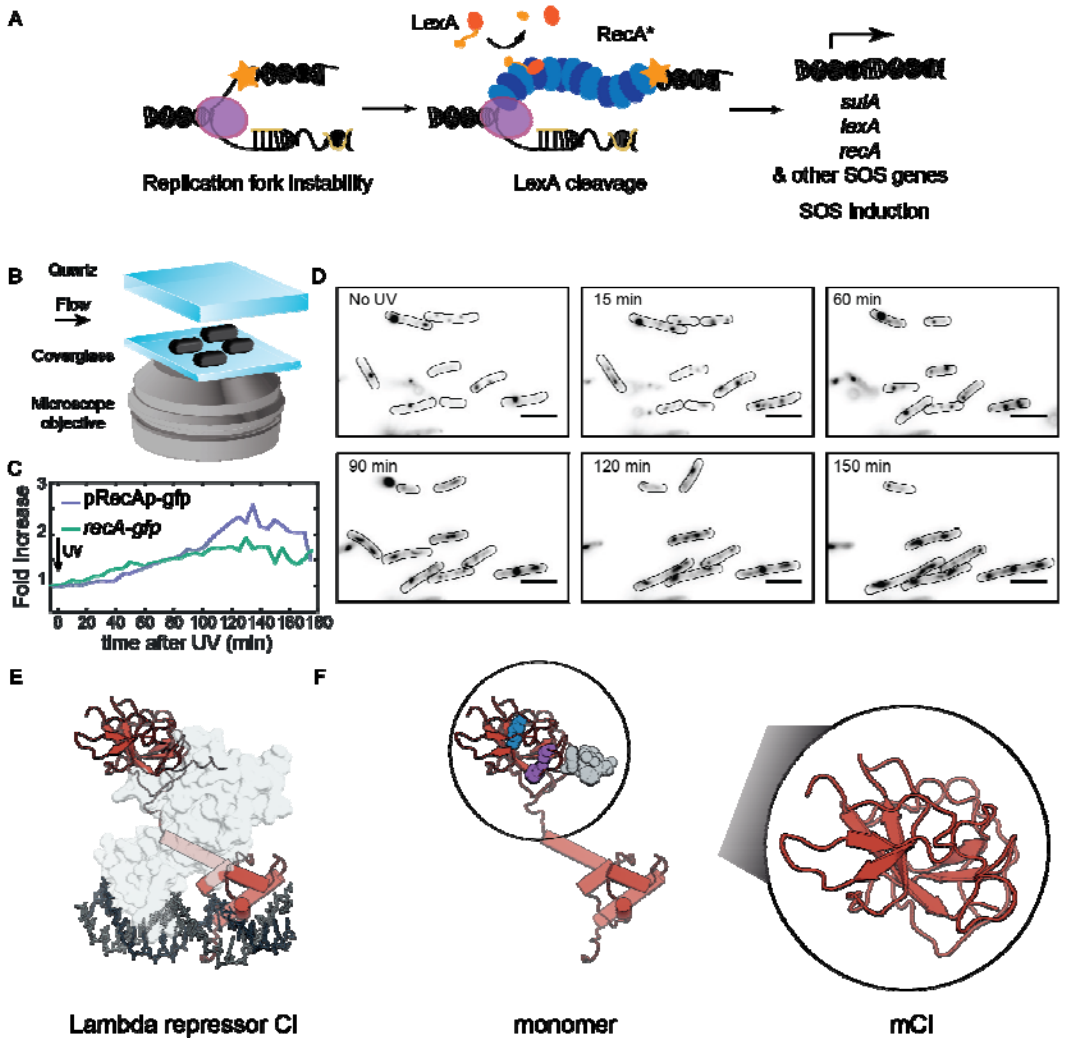

679

680 **Figure 1: RecA forms different intracellular structures in response to UV irradiation**

681 **A.** Consensus model for SOS induction after DNA damage, illustrating the formation of
682 ssDNA-containing RecA* filaments at sites of stalled replication forks. These RecA* filaments
683 induce the SOS response by promoting cleavage of LexA. **B.** Schematic of flow-cell setup for
684 live-cell imaging. **C.** Plots of relative increase in mean intensity of GFP in pRecAp-gfp *cells*
685 (purple, strain# HG260) or RecA-GFP expressed from the native chromosomal locus (*recA-*
686 *gfp* cells). Cells are irradiated with 20 Jm^{-2} of UV at t = 0 min. Shaded error bars represent
687 standard error of the mean cellular fluorescence measured in cells. 50 – 200 cells were
688 analyzed at each time point. Scale bar corresponds to 5 µm. See also SI Movie 1. **D.** Imaging
689 of *recA-gfp* cells (strain# HG195) reveals that RecA-GFP forms foci of various morphologies
690 at different stages during the SOS response. Stills from SI Movie 2 are presented here. **E.**
691 Crystal structure of the operator bound dimeric λ repressor CI (PDB ID: 3BDN). **F.** Monomer
692 of CI showing the catalytic lysine (K192, purple), residues that mediate dimerization (A152

693 and P158, blue), and the C terminus involved in dimerization (grey). Inset shows the
694 monomeric C-terminal fragment 'mCI' defined as CI(101-229, A152T P158A and K192A) used
695 in this study.

696

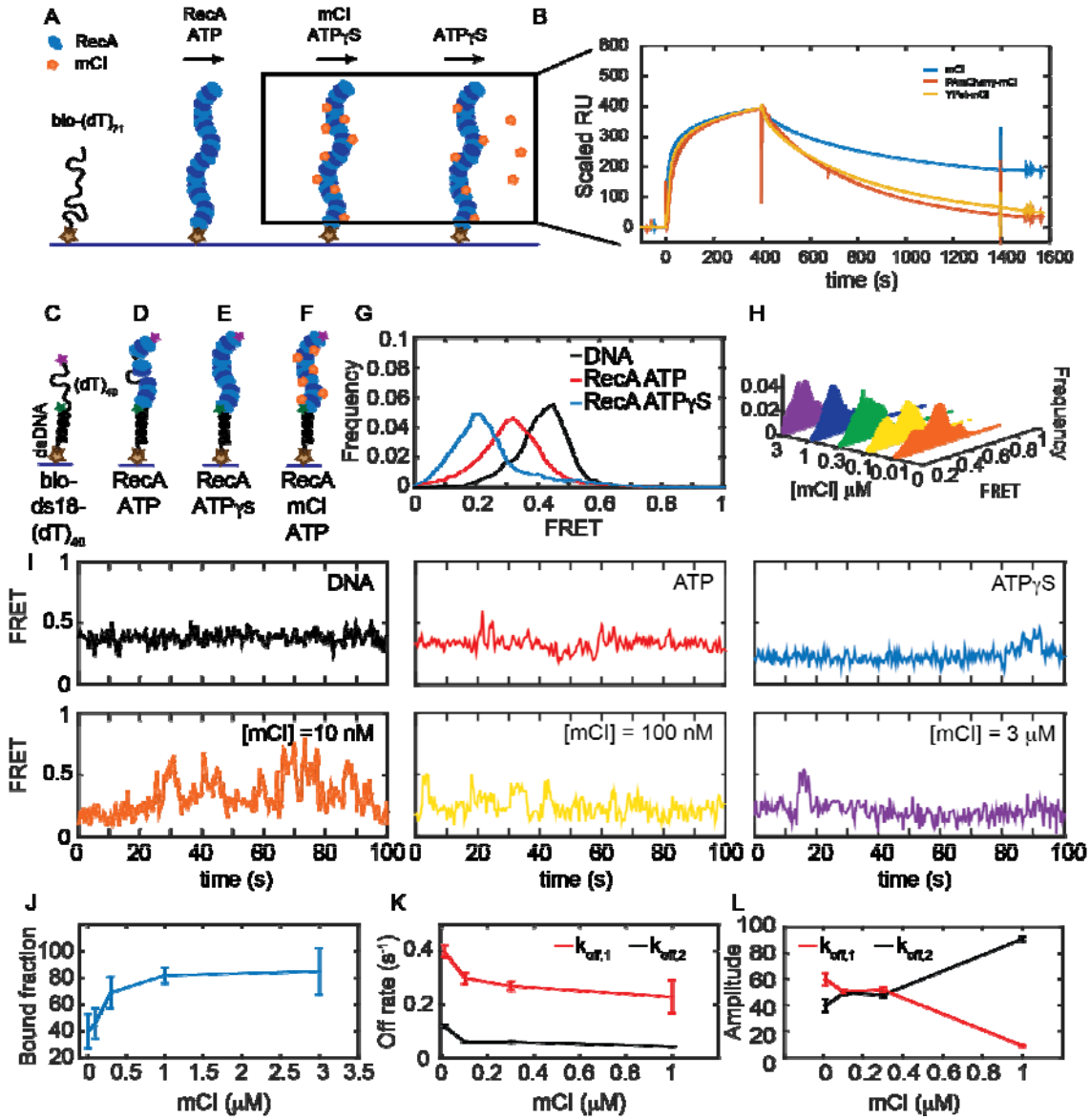

Figure 2: mCI stabilizes ssDNA-RecA filaments *in vitro*

A. Schematic of SPR experiment probing association and dissociation kinetics of mCI from ssDNA-RecA-ATPγS filaments on the surface of an SPR chip. ssDNA-RecA-ATPγS filaments were assembled on a biotinylated $(dT)_{71}$ ssDNA molecule. mCI, YPet-mCI or PAmCherry-mCI were then flowed into the flow cell at time t = 0 for 400 s to monitor the association phase. Dissociation of mCI from ssDNA-RecA-ATPγS filaments was observed by leaving out mCI from the injection buffer. **B.** Sensorgram reveals biphasic association of mCI to RecA filaments, followed by a slow dissociation from the ssDNA-RecA-ATPγS filament. Sensorgrams presented here are corrected for slow disassembly of the RecA-ATPγS filament, and data are scaled to the binding curve of YPet-mCI for purposes of illustration

708 (see also SI Figure 1 for unscaled data). **C.** Schematic of single-molecule FRET assay used to
709 probe the influence of mCI binding on the conformational state of the ssDNA-RecA-ATP
710 filament assembled on a ssDNA $(dT)_{40}$ overhang. Biotinylated substrate DNA (bio-ds18-
711 $(dT)_{40}$) was immobilized on a functionalized coverslip via a streptavidin-biotin interaction. **D.**
712 RecA binds the ssDNA overhang dynamically to form a ssDNA-RecA filament. **E.** In the
713 presence of ATPγS, RecA forms a stable filament. **F.** Incubation with mCI leads to a RecA
714 filament decorated with mCI. **G.** FRET distributions observed from the substrate alone, with
715 RecA-ATP and RecA-ATPγS. **H.** Titration of mCI shifts the RecA-ATP distribution to that of the
716 active filament. **I.** Example FRET traces of DNA substrate alone or when bound to RecA in
717 the presence of ATPγS, or when bound to RecA in the presence of ATP and mCI (0, 10, 100,
718 300, 1000 and 3000 nM mCI) **J.** Fitting of the Hill equation to the percentage of bound
719 fraction as a function [mCI] reveals a K_D of 36 ± 10 nM and a cooperativity of 2.4 ± 0.2 **K.** Off
720 rates measured from binding of mCI to ssDNA-RecA-ATP filaments. **L.** Percentage amplitude
721 of the detected rate-constants as a function of [mCI] reveals enrichment of the population
722 decaying according to the slow off-rate as a function of [mCI]. See also SI Figures 1 and 2.

723

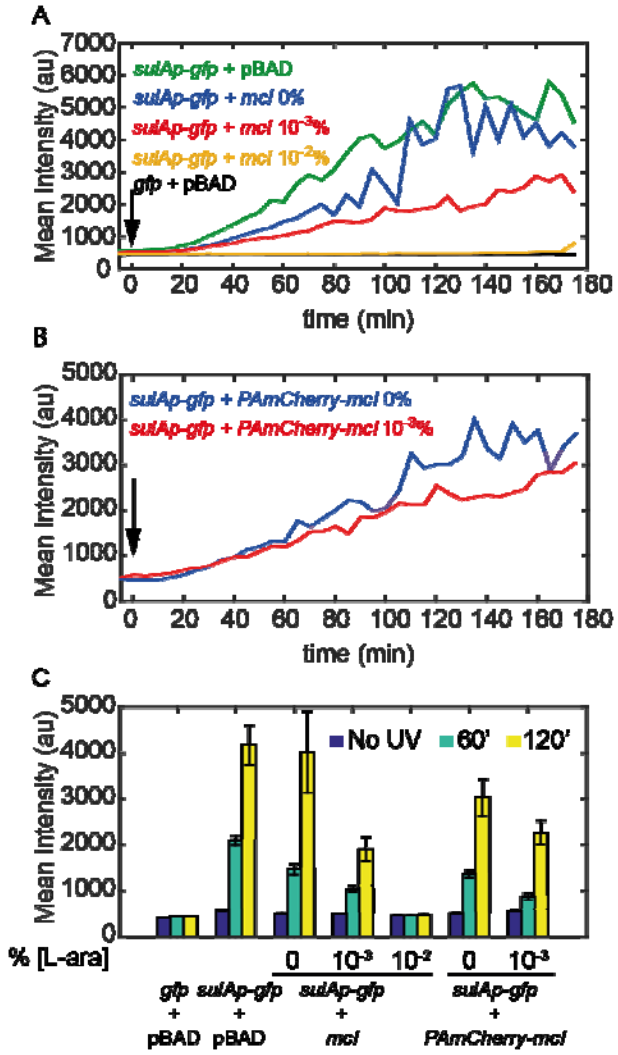

Figure 3: mCI inhibits the SOS response in a concentration-dependent manner

A. Time-lapse experiments were performed on MG1655 cells carrying the SOS-reporter plasmids ('*gfp*' or '*sulAp-gfp*') and pBAD-mCI plasmid ('*mcI*') following irradiation with 20 Jm^{-2} of UV-irradiation at time t = 0 min. Mean intensity of GFP fluorescence was measured in cells carrying the reporter plasmid and mCI or empty vector, and plotted here as follows: '*sulAp-gfp* + pBAD' cells (green; strain# HG258), '*gfp* + pBAD' cells (black; strain# HG257), '*sulAp-gfp* + *mcI*' (strain# HG253) (0% L-ara) (blue), 10^{-3} % L-ara (red) and 10^{-2} % L-ara (yellow), respectively. **B.** Mean intensity of GFP fluorescence in cells carrying the reporter plasmid and pBAD-PAmCherry-mCI plasmid ('*sulAp-gfp* + *PAmCherry-mcI*') (strain# HG285; 0% L-ara (blue) and 10^{-3} % L-ara (red)) is plotted as a function of time. Shaded error bars indicate standard error of mean cellular fluorescence for all cells imaged at the indicated time point. In these experiments, 50-200 cells were analyzed for each experiment for each of the 37 time points. **C.** Bar plots summarizing data presented in B and C under the indicated conditions at a time point before UV irradiation, one at 60, and one at 120 minutes after UV.

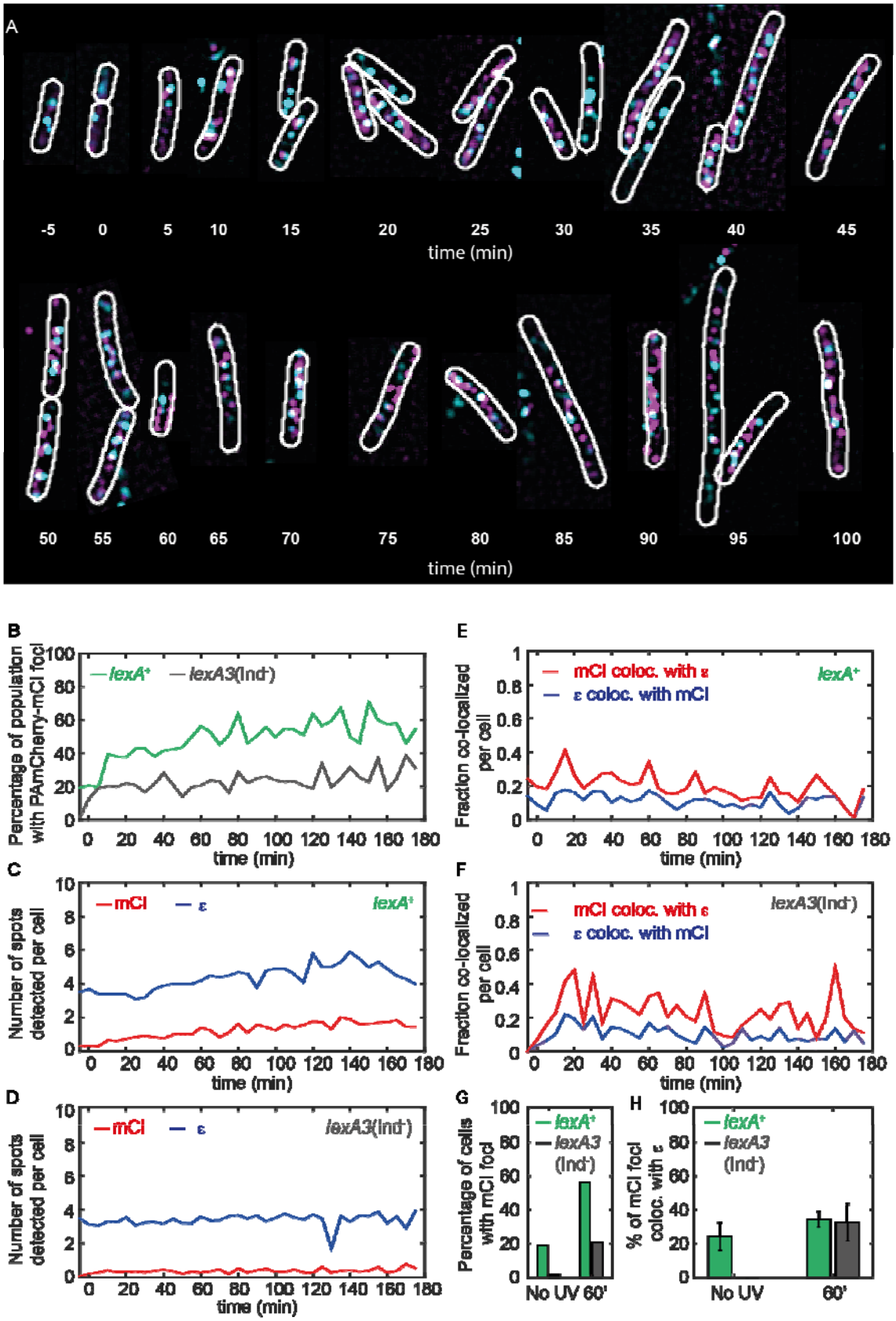

Figure 4: mCI co-localizes with the replisome after UV irradiation

742 MG1655 cells carrying the □-YPet replisome marker and expressing plasmid PAmCherry-mCI
743 from pBAD-PAmCherry-mCI (strain# HG267) were grown in the presence of $5x10^{-4}$ % L-
744 arabinose and irradiated with 20 Jm^{-2} of UV-irradiation followed by imaging for three hours.
745 Examples of **A.** *lexA*$^{+}$ (strain# HG267) provided at indicated time points **B.** The percentage of
746 cells imaged at each time point with at least one PAmCherry-mCI focus is shown for *lexA*$^{+}$
747 (green) and *lexA3*(Ind^{-}) (black) cells. Number of replisome foci and PAmCherry foci were
748 counted for each time point per cell for **C**. *lexA*$^{+}$ and **D**. *lexA3*(Ind^{-}) cells. In cells exhibiting at
749 least one replisome focus and one PAmCherry-mCI focus, the fraction of replisomes co-
750 localizing with PAmCherry-mCI was determined (blue) and the fraction of PAmCherry-mCI
751 co-localizing with replisomes was determined (red) for **E.** *lexA*$^{+}$ and **F.** *lexA3*(Ind^{-}) cells. **G.**
752 Bar plots summarizing percentage of cells exhibiting at least one mCI focus for *lexA*$^{+}$ (green)
753 and *lexA3*(Ind^{-}) (gray) cells before UV and at 60 min after UV irradiation. **H.** Bar plots
754 summarizing extent of co-localization of □-YPet and PAmCherry-mCI in cells with at least one
755 mCI and □ focus. Data are presented as mean ± SEM. 25-150 cells were analyzed for each
756 time point from at least three repeats of each experiment. See also SI Figure 3.

757

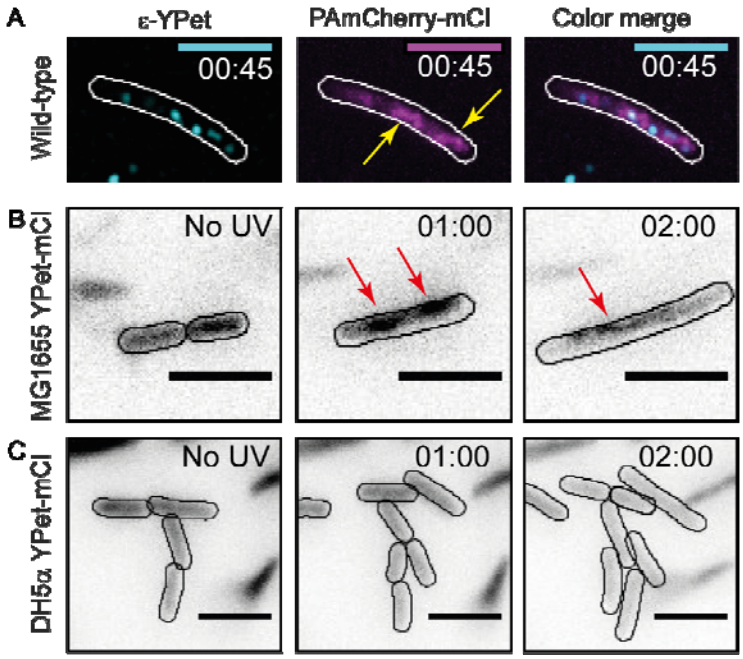

Figure 5: mCI stains RecA bundles after UV-damage

A. At late time points in the DNA damage response, PAmCherry-mCI forms large bundles in *recA*$^{+}$ cells. Shown here is an example of an overlay of the mCI signal (magenta) and replisomal □ foci (cyan) at t = 45 min after 20 Jm^{-2} UV. Yellow arrows point to RecA bundles. For purposes of illustration, peaks in the 514-nm □ channel were enhanced using a discoidal average filter. **B.** YPet-mCI also forms bundles (indicated by red arrows) in response to UV-damage in *recA*$^{+}$ cells. **C.** DH5α carrying the *recA1* allele does not exhibit foci or bundle formation upon UV-irradiation under identical conditions as in panel B. Scale bar corresponds to 5 µm. See also SI Figure 4. Cell outlines provided as a guide to the eye.

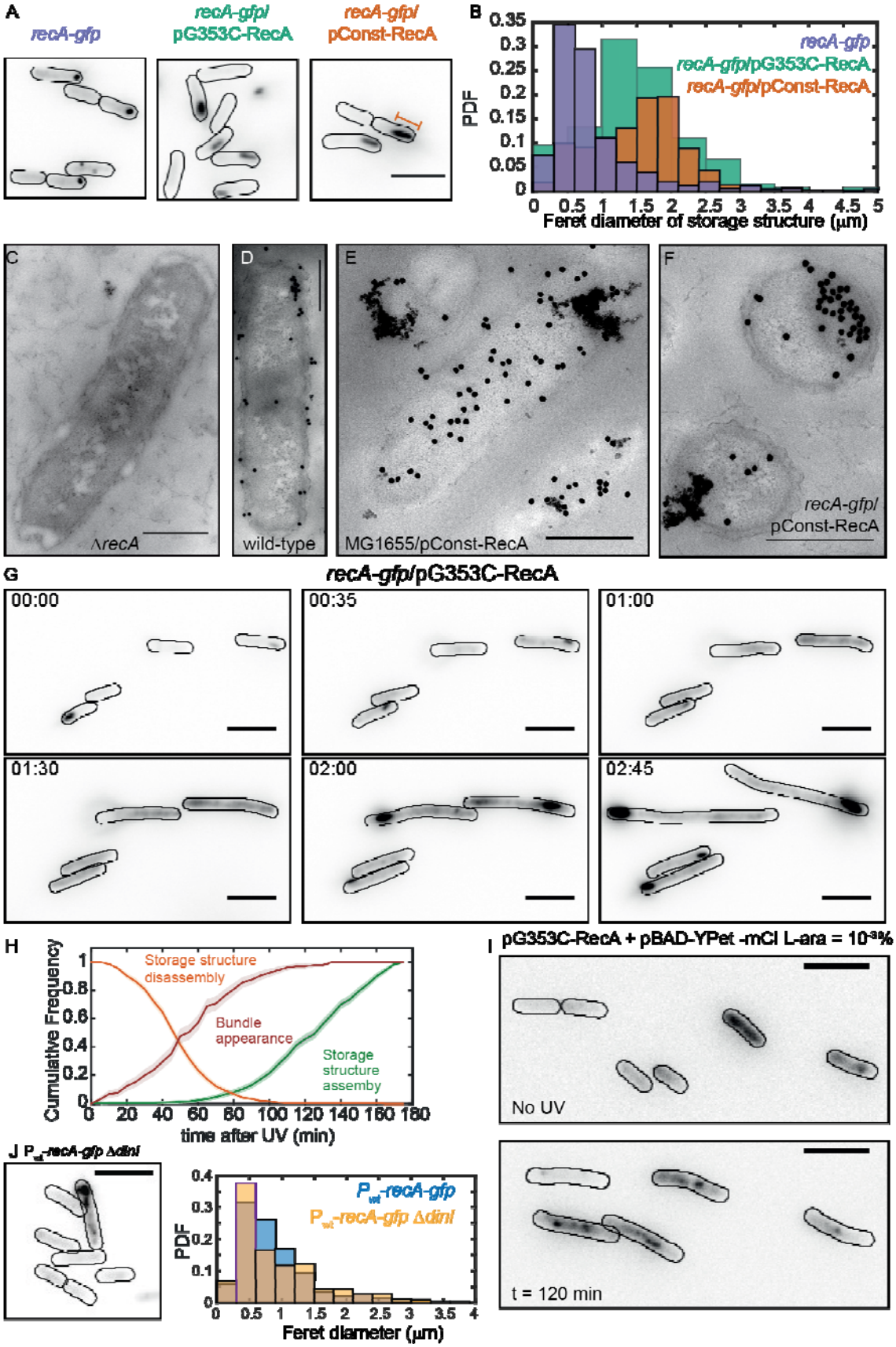

Figure 6: Excess RecA is stored in storage-structures

771 **A.** Montage of *recA-gfp* (strain# HG195), *recA-gfp*/pG353C-RecA (strain# HG406) and *recA-*
772 *gfp*/pConst-RecA cells (strain# HG411) imaged in the absence of UV damage. See also SI
773 Movie 3. **B.** Probability density functions of maximum Feret diameter of storage structures
774 in *recA-gfp* (purple), *recA-gfp*/pG353C-RecA (green) and *recA-gfp*/pConst-RecA (orange)
775 cells. Orange bar in panel A represents the maximum Feret diameter for that particular
776 storage structure. Electron microscopy images of **C**. Δ*recA* **D**. wild-type *recA* **E**. *recA-*
777 *gfp*/pConst-RecA and **F**. MG1655/pConst-RecA cells stained with gold nanoparticles labelled
778 with RecA antibody. Note the appearance of aggregates of gold nanoparticles at locations
779 consistent with those observed in panel A for *recA-gfp*/pConst-RecA cells (panel E).
780 Untagged, over-expressed RecA (F) reveals gold nanoparticle localizations consistent with
781 those expected from RecA storage structures. Scale bar corresponds to 1 µm. **G.** Montage of
782 frames from a time-lapse experiment of *recA-gfp*/pG353C-RecA cells exposed to UV (see
783 also SI Movies 3 and 4). RecA forms storage structures in the absence of DNA damage (0
784 min) in cells. Storage structures dynamically dissolve after DNA damage (1 h). Storage
785 structures reform by sequestering excess RecA synthesized during SOS after repair (2 h and
786 2 h 45 min time points). **H.** Cumulative probability distributions of time of solubilization of
787 storage structure (yellow) and time of appearance (light green) of storage structures from
788 *recA-gfp*/pG353C-RecA (strain# HG406) cells. Red line represents cumulative probability
789 distribution of time of first incidence of RecA bundles in *recA-gfp* cells (strain# HG195).
790 Shaded error bars represent standard deviation of the bootstrap distribution obtained by
791 sampling 80% of the data 1,000 times. In each case, 100-150 cells were analyzed that were
792 present for the duration of observation (3 h). Scale bar represents 5 µm. **I.** YPet-mCI does
793 not stain storage structures in MG1655/pG353C-RecA pBAD-Ypet-mCI cells (strain# HG446)
794 in the absence of DNA damage, but forms features after UV damage (shown here is a still at
795 120 min). Cell outlines provided as a guide to the eye. See also SI Movie 5, and SI Figure 5. **J.**
796 MG1655 cells carrying the *recA-gfp* fusion under the native *recA* promoter and Δ*dinI* (strain#
797 EAW 767) exhibit fewer, and smaller storage structures than *dinI*$^{+}$ cells.

798

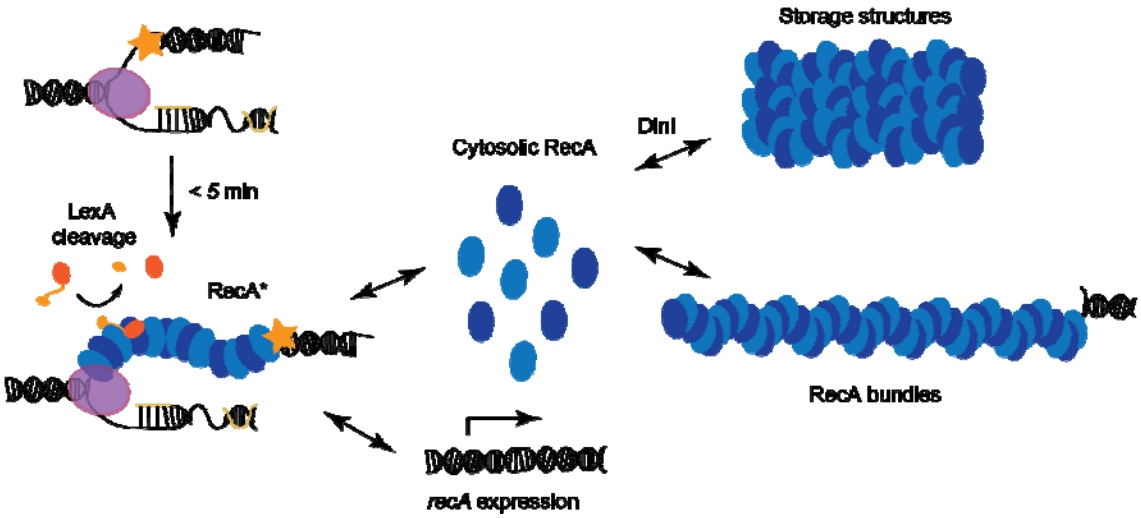

Figure 7: Model for organization of RecA complexes after DNA damage

Model for storage and re-distribution of RecA after DNA damage. Detection of UV damage leads to formation of ssDNA-RecA filaments at sites of replisomes. These ssDNA-RecA filaments catalyze auto-proteolysis of LexA to induce SOS and upregulate expression of RecA. Storage structures of RecA dissolve in response to DNA damage to make RecA available for repair and recombination.

806 **References**

807 Baumann, P., Benson, F.E., and West, S.C. (1996). Human Rad51 protein promotes ATP-dependent
808 homologous pairing and strand transfer reactions in vitro. Cell *87*, 757-766.
809 Bianco, P.R., Tracy, R.B., and Kowalczykowski, S.C. (1998). DNA strand exchange proteins: a
810 biochemical and physical comparison. Front Biosci *3*, D570-603.
811 Boudsocq, F., Campbell, M., Devoret, R., and Bailone, A. (1997). Quantitation of the inhibition of Hfr
812 x F- recombination by the mutagenesis complex UmuD'C. J Mol Biol *270*, 201-211.
813 Brenner, S.L., Zlotnick, A., and Griffith, J.D. (1988). RecA protein self-assembly. Multiple discrete
814 aggregation states. J Mol Biol *204*, 959-972.
815 Bryant, F.R. (1988). Construction of a recombinase-deficient mutant recA protein that retains single-
816 stranded DNA-dependent ATPase activity. J Biol Chem *263*, 8716-8723.
817 Burckhardt, S.E., Woodgate, R., Scheuermann, R.H., and Echols, H. (1988). UmuD mutagenesis
818 protein of Escherichia coli: overproduction, purification, and cleavage by RecA. Proc Natl Acad Sci U S
819 A *85*, 1811-1815.
820 Centore, R.C., and Sandler, S.J. (2007). UvrD limits the number and intensities of RecA-green
821 fluorescent protein structures in Escherichia coli K-12. Journal of bacteriology *189*, 2915-2920.
822 Chen, J., Morrical, M.D., Donigan, K.A., Weidhaas, J.B., Sweasy, J.B., Averill, A.M., Tomczak, J.A., and
823 Morrical, S.W. (2015). Tumor-associated mutations in a conserved structural motif alter physical and
824 biochemical properties of human RAD51 recombinase. Nucleic Acids Res *43*, 1098-1111.
825 Cohen, S., Knoll, B.J., Little, J.W., and Mount, D.W. (1981). Preferential cleavage of phage lambda
826 repressor monomers by recA protease. Nature *294*, 182-184.
827 Courcelle, J., Khodursky, A., Peter, B., Brown, P.O., and Hanawalt, P.C. (2001). Comparative gene
828 expression profiles following UV exposure in wild-type and SOS-deficient Escherichia coli. Genetics
829 *158*, 41-64.
830 Cox, M.M. (2007). Regulation of bacterial RecA protein function. Crit Rev Biochem Mol Biol *42*, 41-
831 63.
832 Cox, M.M., Goodman, M.F., Kreuzer, K.N., Sherratt, D.J., Sandler, S.J., and Marians, K.J. (2000). The
833 importance of repairing stalled replication forks. Nature *404*, 37-41.
834 Craig, N.L., and Roberts, J.W. (1981). Function of nucleoside triphosphate and polynucleotide in
835 Escherichia coli recA protein-directed cleavage of phage lambda repressor. J Biol Chem *256*, 8039-
836 8044.
837 Echols, H., and Green, L. (1971). Establishment and maintenance of repression by bacteriophage
838 lambda: the role of the cI, cII, and c3 proteins. Proc Natl Acad Sci U S A *68*, 2190-2194.
839 Egelman, E.H., and Stasiak, A. (1986). Structure of helical RecA-DNA complexes. Complexes formed
840 in the presence of ATP-gamma-S or ATP. J Mol Biol *191*, 677-697.
841 Egelman, E.H., and Stasiak, A. (1988). Structure of helical RecA-DNA complexes. II. Local
842 conformational changes visualized in bundles of RecA-ATP gamma S filaments. J Mol Biol *200*, 329-
843 349.
844 Eggler, A.L., Lusetti, S.L., and Cox, M.M. (2003). The C terminus of the Escherichia coli RecA protein
845 modulates the DNA binding competition with single-stranded DNA-binding protein. J Biol Chem *278*,
846 16389-16396.
847 Ferentz, A.E., Opperman, T., Walker, G.C., and Wagner, G. (1997). Dimerization of the UmuD' protein
848 in solution and its implications for regulation of SOS mutagenesis. Nat Struct Biol *4*, 979-983.
849 Fernandez De Henestrosa, A.R., Ogi, T., Aoyagi, S., Chafin, D., Hayes, J.J., Ohmori, H., and Woodgate,
850 R. (2000). Identification of additional genes belonging to the LexA regulon in Escherichia coli. Mol
851 Microbiol *35*, 1560-1572.
852 Frank, E.G., Cheng, N., Do, C.C., Cerritelli, M.E., Bruck, I., Goodman, M.F., Egelman, E.H., Woodgate,
853 R., and Steven, A.C. (2000). Visualization of two binding sites for the Escherichia coli UmuD'(2)C
854 complex (DNA pol V) on RecA-ssDNA filaments. J Mol Biol *297*, 585-597.

855 Galkin, V.E., Yu, X., Bielnicki, J., Ndjonka, D., Bell, C.E., and Egelman, E.H. (2009). Cleavage of
856 bacteriophage lambda cI repressor involves the RecA C-terminal domain. J Mol Biol *385*, 779-787.
857 Garvey, N., St John, A.C., and Witkin, E.M. (1985). Evidence for RecA protein association with the cell
858 membrane and for changes in the levels of major outer membrane proteins in SOS-induced
859 Escherichia coli cells. Journal of bacteriology *163*, 870-876.
860 Ghodke, H., Caldas, V.E., Punter, C.M., van Oijen, A.M., and Robinson, A. (2016). Single-Molecule
861 Specific Mislocalization of Red Fluorescent Proteins in Live Escherichia coli. Biophys J *111*, 25-27.
862 Gimble, F.S., and Sauer, R.T. (1985). Mutations in bacteriophage lambda repressor that prevent
863 RecA-mediated cleavage. Journal of bacteriology *162*, 147-154.
864 Gimble, F.S., and Sauer, R.T. (1989). Lambda repressor mutants that are better substrates for RecA-
865 mediated cleavage. J Mol Biol *206*, 29-39.
866 Guzman, L.M., Belin, D., Carson, M.J., and Beckwith, J. (1995). Tight regulation, modulation, and
867 high-level expression by vectors containing the arabinose PBAD promoter. Journal of bacteriology
868 *177*, 4121-4130.
869 Handa, N., Amitani, I., Gumlaw, N., Sandler, S.J., and Kowalczykowski, S.C. (2009). Single molecule
870 analysis of a red fluorescent RecA protein reveals a defect in nucleoprotein filament nucleation that
871 relates to its reduced biological functions. J Biol Chem *284*, 18664-18673.
872 Henrikus, S.S., Wood, E.A., McDonald, J.P., Cox, M.M., Woodgate, R., Goodman, M.F., van Oijen,
873 A.M., and Robinson, A. (2018). DNA polymerase IV primarily operates outside of DNA replication
874 forks in Escherichia coli. PLoS genetics *14*, e1007161.
875 Howard-Flanders, P., Rupp, W.D., Wilkins, B.M., and Cole, R.S. (1968). DNA replication and
876 recombination after UV irradiation. Cold Spring Harb Symp Quant Biol *33*, 195-207.
877 Jaszczur, M., Bertram, J.G., Robinson, A., van Oijen, A.M., Woodgate, R., Cox, M.M., and Goodman,
878 M.F. (2016). Mutations for Worse or Better: Low-Fidelity DNA Synthesis by SOS DNA Polymerase V Is
879 a Tightly Regulated Double-Edged Sword. Biochemistry *55*, 2309-2318.
880 Jiang, Q., Karata, K., Woodgate, R., Cox, M.M., and Goodman, M.F. (2009). The active form of DNA
881 polymerase V is UmuD'(2)C-RecA-ATP. Nature *460*, 359-363.
882 Kalir, S., McClure, J., Pabbaraju, K., Southward, C., Ronen, M., Leibler, S., Surette, M.G., and Alon, U.
883 (2001). Ordering genes in a flagella pathway by analysis of expression kinetics from living bacteria.
884 Science *292*, 2080-2083.
885 Kato, M., Yano, K., Matsuo, F., Saito, H., Katagiri, T., Kurumizaka, H., Yoshimoto, M., Kasumi, F.,
886 Akiyama, F., Sakamoto, G., *et al.* (2000). Identification of Rad51 alteration in patients with bilateral
887 breast cancer. J Hum Genet *45*, 133-137.
888 Kenyon, C.J., and Walker, G.C. (1980). DNA-damaging agents stimulate gene expression at specific
889 loci in Escherichia coli. Proc Natl Acad Sci U S A *77*, 2819-2823.
890 Kidane, D., and Graumann, P.L. (2005). Dynamic formation of RecA filaments at DNA double strand
891 break repair centers in live cells. J Cell Biol *170*, 357-366.
892 Kim, T., Chitteni-Pattu, S., Cox, B.L., Wood, E.A., Sandler, S.J., and Cox, M.M. (2015). Directed
893 Evolution of RecA Variants with Enhanced Capacity for Conjugational Recombination. PLoS genetics
894 *11*, e1005278.
895 Kowalczykowski, S.C. (2000). Initiation of genetic recombination and recombination-dependent
896 replication. Trends Biochem Sci *25*, 156-165.
897 Kuzminov, A. (1995). Collapse and repair of replication forks in Escherichia coli. Mol Microbiol *16*,
898 373-384.
899 Lenhart, J.S., Brandes, E.R., Schroeder, J.W., Sorenson, R.J., Showalter, H.D., and Simmons, L.A.
900 (2014). RecO and RecR are necessary for RecA loading in response to DNA damage and replication
901 fork stress. Journal of bacteriology *196*, 2851-2860.
902 Lesterlin, C., Ball, G., Schermelleh, L., and Sherratt, D.J. (2014). RecA bundles mediate homology
903 pairing between distant sisters during DNA break repair. Nature *506*, 249-253.
904 Lestini, R., and Michel, B. (2007). UvrD controls the access of recombination proteins to blocked
905 replication forks. EMBO J *26*, 3804-3814.

906 Levin-Zaidman, S., Frenkiel-Krispin, D., Shimoni, E., Sabanay, I., Wolf, S.G., and Minsky, A. (2000).
907 Ordered intracellular RecA-DNA assemblies: a potential site of in vivo RecA-mediated activities. Proc
908 Natl Acad Sci U S A *97*, 6791-6796.
909 Little, J.W. (1982). Control of the SOS regulatory system by the level of RecA protease. Biochimie *64*,
910 585-589.
911 Little, J.W., and Mount, D.W. (1982). The SOS regulatory system of Escherichia coli. Cell *29*, 11-22.
912 Little, J.W., Mount, D.W., and Yanisch-Perron, C.R. (1981). Purified lexA protein is a repressor of the
913 recA and lexA genes. Proc Natl Acad Sci U S A *78*, 4199-4203.
914 Luo, Y., Pfuetzner, R.A., Mosimann, S., Paetzel, M., Frey, E.A., Cherney, M., Kim, B., Little, J.W., and
915 Strynadka, N.C. (2001). Crystal structure of LexA: a conformational switch for regulation of self-
916 cleavage. Cell *106*, 585-594.
917 Lusetti, S.L., and Cox, M.M. (2002). The bacterial RecA protein and the recombinational DNA repair
918 of stalled replication forks. Annu Rev Biochem *71*, 71-100.
919 Lusetti, S.L., Drees, J.C., Stohl, E.A., Seifert, H.S., and Cox, M.M. (2004a). The DinI and RecX proteins
920 are competing modulators of RecA function. J Biol Chem *279*, 55073-55079.
921 Lusetti, S.L., Shaw, J.J., and Cox, M.M. (2003a). Magnesium ion-dependent activation of the RecA
922 protein involves the C terminus. J Biol Chem *278*, 16381-16388.
923 Lusetti, S.L., Voloshin, O.N., Inman, R.B., Camerini-Otero, R.D., and Cox, M.M. (2004b). The DinI
924 protein stabilizes RecA protein filaments. J Biol Chem *279*, 30037-30046.
925 Lusetti, S.L., Wood, E.A., Fleming, C.D., Modica, M.J., Korth, J., Abbott, L., Dwyer, D.W., Roca, A.I.,
926 Inman, R.B., and Cox, M.M. (2003b). C-terminal deletions of the Escherichia coli RecA protein.
927 Characterization of in vivo and in vitro effects. J Biol Chem *278*, 16372-16380.
928 Markham, B.E., Little, J.W., and Mount, D.W. (1981). Nucleotide sequence of the lexA gene of
929 Escherichia coli K-12. Nucleic Acids Res *9*, 4149-4161.
930 Ndjonka, D., and Bell, C.E. (2006). Structure of a hyper-cleavable monomeric fragment of phage
931 lambda repressor containing the cleavage site region. J Mol Biol *362*, 479-489.
932 Ouzounov, N., Nguyen, J.P., Bratton, B.P., Jacobowitz, D., Gitai, Z., and Shaevitz, J.W. (2016). MreB
933 Orientation Correlates with Cell Diameter in Escherichia coli. Biophys J *111*, 1035-1043.
934 Park, J., Myong, S., Niedziela-Majka, A., Lee, K.S., Yu, J., Lohman, T.M., and Ha, T. (2010). PcrA
935 helicase dismantles RecA filaments by reeling in DNA in uniform steps. Cell *142*, 544-555.
936 Petrova, V., Chen, S.H., Molzberger, E.T., Tomko, E., Chitteni-Pattu, S., Jia, H., Ordabayev, Y., Lohman,
937 T.M., and Cox, M.M. (2015). Active displacement of RecA filaments by UvrD translocase activity.
938 Nucleic Acids Res *43*, 4133-4149.
939 Prakash, R., Zhang, Y., Feng, W., and Jasin, M. (2015). Homologous recombination and human
940 health: the roles of BRCA1, BRCA2, and associated proteins. Cold Spring Harb Perspect Biol *7*,
941 a016600.
942 Ptashne, M., Jeffrey, A., Johnson, A.D., Maurer, R., Meyer, B.J., Pabo, C.O., Roberts, T.M., and Sauer,
943 R.T. (1980). How the lambda repressor and cro work. Cell *19*, 1-11.
944 Rajendram, M., Zhang, L., Reynolds, B.J., Auer, G.K., Tuson, H.H., Ngo, K.V., Cox, M.M., Yethiraj, A.,
945 Cui, Q., and Weibel, D.B. (2015). Anionic Phospholipids Stabilize RecA Filament Bundles in
946 Escherichia coli. Mol Cell *60*, 374-384.
947 Ramirez, B.E., Voloshin, O.N., Camerini-Otero, R.D., and Bax, A. (2000). Solution structure of DinI
948 provides insight into its mode of RecA inactivation. Protein Sci *9*, 2161-2169.
949 Renzette, N., Gumlaw, N., Nordman, J.T., Krieger, M., Yeh, S.P., Long, E., Centore, R., Boonsombat,
950 R., and Sandler, S.J. (2005). Localization of RecA in Escherichia coli K-12 using RecA-GFP. Mol
951 Microbiol *57*, 1074-1085.
952 Renzette, N., Gumlaw, N., and Sandler, S.J. (2007). DinI and RecX modulate RecA-DNA structures in
953 Escherichia coli K-12. Mol Microbiol *63*, 103-115.
954 Reyes-Lamothe, R., Sherratt, D.J., and Leake, M.C. (2010). Stoichiometry and architecture of active
955 DNA replication machinery in Escherichia coli. Science *328*, 498-501.

956 Roberts, J.W., and Roberts, C.W. (1975). Proteolytic cleavage of bacteriophage lambda repressor in
957 induction. Proc Natl Acad Sci U S A *72*, 147-151.
958 Robinson, A., McDonald, J.P., Caldas, V.E., Patel, M., Wood, E.A., Punter, C.M., Ghodke, H., Cox,
959 M.M., Woodgate, R., Goodman, M.F.*, et al.* (2015). Regulation of Mutagenic DNA Polymerase V
960 Activation in Space and Time. PLoS genetics *11*, e1005482.
961 Ronen, M., Rosenberg, R., Shraiman, B.I., and Alon, U. (2002). Assigning numbers to the arrows:
962 parameterizing a gene regulation network by using accurate expression kinetics. Proc Natl Acad Sci U
963 S A *99*, 10555-10560.
964 Rupp, W.D., and Howard-Flanders, P. (1968). Discontinuities in the DNA synthesized in an excision-
965 defective strain of Escherichia coli following ultraviolet irradiation. J Mol Biol *31*, 291-304.
966 Salles, B., and Paoletti, C. (1983). Control of UV induction of recA protein. Proc Natl Acad Sci U S A
967 *80*, 65-69.
968 San Filippo, J., Sung, P., and Klein, H. (2008). Mechanism of eukaryotic homologous recombination.
969 Annu Rev Biochem *77*, 229-257.
970 Sassanfar, M., and Roberts, J.W. (1990). Nature of the SOS-inducing signal in Escherichia coli. The
971 involvement of DNA replication. J Mol Biol *212*, 79-96.
972 Sauer, R.T., Ross, M.J., and Ptashne, M. (1982). Cleavage of the lambda and P22 repressors by recA
973 protein. J Biol Chem *257*, 4458-4462.
974 Stasiak, A., and Egelman, E.H. (1986). Structure and Dynamics of recA Protein-DNA Complexes as
975 Determined by Image Analysis of Electron Micrographs. Biophys J *49*, 5-7.
976 Stayrook, S., Jaru-Ampornpan, P., Ni, J., Hochschild, A., and Lewis, M. (2008). Crystal structure of the
977 lambda repressor and a model for pairwise cooperative operator binding. Nature *452*, 1022-1025.
978 Stohl, E.A., Brockman, J.P., Burkle, K.L., Morimatsu, K., Kowalczykowski, S.C., and Seifert, H.S. (2003).
979 Escherichia coli RecX inhibits RecA recombinase and coprotease activities in vitro and in vivo. J Biol
980 Chem *278*, 2278-2285.
981 Sung, P. (1994). Catalysis of ATP-dependent homologous DNA pairing and strand exchange by yeast
982 RAD51 protein. Science *265*, 1241-1243.
983 Uhlin, B.E., Volkert, M.R., Clark, A.J., Sancar, A., and Rupp, W.D. (1982). Nucleotide sequence of a
984 recA operator mutation. LexA/operator-repressor binding/inducible repair. Mol Gen Genet *185*, 251-
985 254.
986 Veaute, X., Delmas, S., Selva, M., Jeusset, J., Le Cam, E., Matic, I., Fabre, F., and Petit, M.A. (2005).
987 UvrD helicase, unlike Rep helicase, dismantles RecA nucleoprotein filaments in Escherichia coli.
988 EMBO J *24*, 180-189.
989 Volkert, M.R., George, D.L., and Witkin, E.M. (1976). Partial suppression of the LexA phenotype by
990 mutations (rnm) which restore ultraviolet resistance but not ultraviolet mutability to Escherichia coli
991 B/r uvr A lexA. Mutat Res *36*, 17-28.
992 Walker, G.C. (2001). To cleave or not to cleave? Insights from the LexA crystal structure. Mol Cell *8*,
993 486-487.
994 Yeeles, J.T., and Marians, K.J. (2013). Dynamics of leading-strand lesion skipping by the replisome.
995 Mol Cell *52*, 855-865.
996 Yu, X., and Egelman, E.H. (1993). The LexA repressor binds within the deep helical groove of the
997 activated RecA filament. J Mol Biol *231*, 29-40.
998 Zaslaver, A., Bren, A., Ronen, M., Itzkovitz, S., Kikoin, I., Shavit, S., Liebermeister, W., Surette, M.G.,
999 and Alon, U. (2006). A comprehensive library of fluorescent transcriptional reporters for Escherichia
1000 coli. Nat Methods *3*, 623-628.

1001